Cellular and Molecular Neurobiology
https://doi.org/10.1007/s10571-022-01268-7

ORIGINAL RESEARCH

Dietary Fiber Modulates the Release of Gut Bacterial Products Preventing Cognitive Decline in an Alzheimer's Mouse Model

Daniel Cuervo-Zanatta[1,2] · Tauqeerunnisa Syeda[1] · Vicente Sánchez-Valle[1] · Mariangel Irene-Fierro[1] · Pablo Torres-Aguilar[3] · Mónica Adriana Torres-Ramos[3] · Mineko Shibayama-Salas[4] · Angélica Silva-Olivares[4] · Lilia G. Noriega[5] · Nimbe Torres[5] · Armando R. Tovar[5] · Iván Ruminot[6] · L. Felipe Barros[6] · Jaime García-Mena[2] · Claudia Perez-Cruz[1]

Received: 13 April 2022 / Accepted: 28 July 2022

Abstract

Fiber intake is associated with a lower risk for Alzheimer´s disease (AD) in older adults. Intake of plant-based diets rich in soluble fiber promotes the production of short-chain fatty acids (SCFAs: butyrate, acetate, propionate) by gut bacteria. Butyrate administration has antiinflammatory actions, but propionate promotes neuroinflammation. In AD patients, gut microbiota dysbiosis is a common feature even in the prodromal stages of the disease. It is unclear whether the neuroprotective effects of fiber intake rely on gut microbiota modifications and specific actions of SCFAs in brain cells. Here, we show that restoration of the gut microbiota dysbiosis through the intake of soluble fiber resulted in lower propionate and higher butyrate production, reduced astrocyte activation and improved cognitive function in 6-month-old male APP/PS1 mice. The neuroprotective effects were lost in antibiotic-treated mice. Moreover, propionate promoted higher glycolysis and mitochondrial respiration in astrocytes, while butyrate induced a more quiescent metabolism. Therefore, fiber intake neuroprotective action depends on the modulation of butyrate/propionate production by gut bacteria. Our data further support and provide a mechanism to explain the beneficial effects of dietary interventions rich in soluble fiber to prevent dementia and AD.

Graphical Abstract

Fiber intake restored the concentration of propionate and butyrate by modulating the composition of gut microbiota in male transgenic (Tg) mice with Alzheimer´s disease. Gut dysbiosis was associated with intestinal damage and high propionate levels in control diet fed-Tg mice. Fiber-rich diet restored intestinal integrity and promoted the abundance of butyrate-producing bacteria. Butyrate concentration was associated with better cognitive performance in fiber-fed Tg mice. A fiber-rich diet may

✉ Jaime García-Mena
jgmena@cinvestav.mx

✉ Claudia Perez-Cruz
cperezc@cinvestav.mx

[1] Laboratorio de Neuroplasticidad y Neurodegeneración, Departamento de Farmacologia, Centro de Investigación y de Estudios Avanzados del I.P.N. (Cinvestav), Av. IPN 2508, Ciudad de Mexico 07360, México

[2] Laboratorio de Referencia y Soporte Para Genomas, Transcriptomas y Caracterización de Microbiomas, Departamento de Genética y Biología Molecular, Centro de Investigación y de Estudios Avanzados del I.P.N. (Cinvestav), Av. IPN 2508, Ciudad de Mexico 07360, México

[3] Unidad Periférica de Neurociencias, Instituto de Neurología y Neurocirugía Manuel Velasco Suárez (INNNMVS), Ciudad de Mexico 14269, México

[4] Departmento de Infectómica y Patogénesis Molecular, Centro de Investigación y de Estudios Avanzados del I.P.N. (Cinvestav), Av. IPN 2508, 07360 Ciudad de Mexico, Mexico

[5] Departamento de Fisiología de la Nutrición, Instituto Nacional de Ciencias Médicas y de la Nutrición "Salvador Zubiran" (INCMNSZ), 14080 Ciudad de México, Mexico

[6] Universidad San Sebastián, Facultad de Medicina y Ciencia, Centro de Estudios Científicos-CECs, Valdivia, Chile

Published online: 11 August 2022

prevent the development of a dysbiotic microbiome and the related cognitive dysfunction in people at risk of developing Alzheimer´s disease.

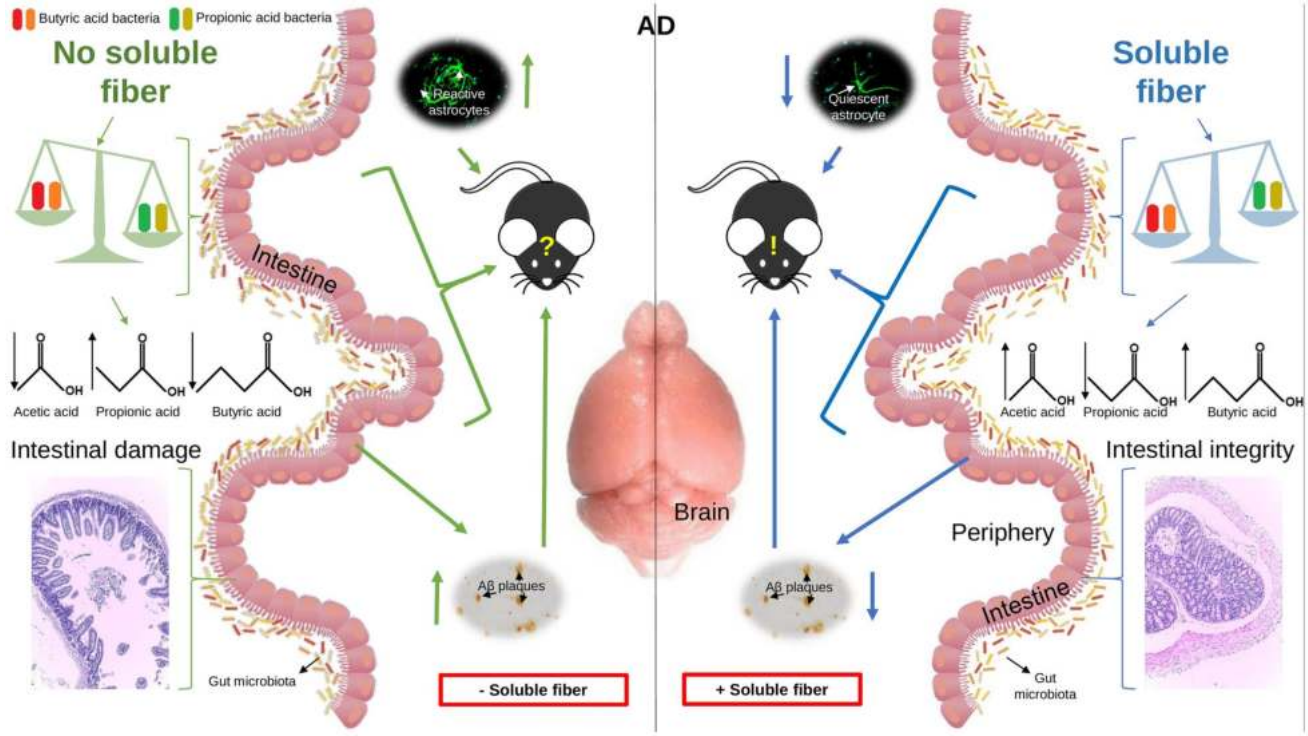

Introduction

Alzheimer's disease (AD) is a neurological disorder characterized by progressive memory decline and cognitive impairment. Amyloid-beta (Aβ) aggregation, hyperphosphorylation of tau, and gliosis are the major histopathological hallmarks of AD (Akiyama et al. 2000; Khandelwal et al. 2011; Engelhart et al. 2004; Guo et al. 2006). It has been estimated that up to a third of all AD cases can be prevented if the modifiable lifestyle risk factors are avoided (Norton et al. 2014). Diet is a modifiable lifestyle factor that can protect against cognitive impairment and dementia (Yusufov et al. 2017). A higher adherence to the MeDi diet slows the progression from Mild Cognitive Impairment (MCI) to AD and reduces the risk of developing MCI and dementia (Singh et al. 2014; Morris 2016). High adherence to MeDi diet is associated with lower mortality in AD patients (Scarmeas et al. 2007; Solfrizzi et al. 2010). Macro- and micronutrients content in MeDi diet are difficult to determine to understand the nutritional patterns for AD prevention (Morris 2016). However, only the consumption of vegetables, especially green leafy vegetables, cause an inverse association with cognitive decline (Trichopoulou et al. 2015). Green vegetables are food with a high fiber content (Anderson 1990). Soluble fibers can be considered as prebiotic, a substrate that is selectively utilized by host microorganisms conferring a health benefit (Gibson et al. 2017). Prebiotics can reshape the gut microbiota (GM) and enhance the abundance of bacteria with essential health benefits (Guan et al. 2021); this is important in AD research as alterations in the GM have been widely reported in AD and MCI subjects (Liu et al. 2019; Lu et al. 2019; Cattaneo et al. 2017; Vogt 1995). Therefore, this study aimed to evaluate the impact of fiber intake, as a key player in the microbiota-brain axis, against Aβ aggregation, inflammation and cognitive function in an AD mice model.

Short-chain fatty acids (SCFAs) are the most studied bacterial fermentation products after soluble fiber intake (Dalile et al. 2019); acetate, propionate, and butyrate are the major bacterial products in the colon (Macfarlane and Macfarlane 2003). SCFAs can be released into the bloodstream and reach the brain (Bélanger et al. 2011; Dalile et al. 2019; Vijay and Morris 2014). Despite the only one-carbon difference in their molecule structure, propionate and butyrate exert opposite effects in brain cells. Intracerebroventricular infusions of propionate disturb fatty acid metabolism

(Abdelli et al. 2019; MacFabe 2015; Shultz et al. 2008) and cause astrocyte activation (De Almeida et al. 2006). In contrast, butyrate exerts anti-inflammatory effects (Segain et al. 2000), reducing GFAP expression in astrocytes (Kanski et al. 2014), reversing learning deficits, and restoring dendritic spine density in hippocampal neurons of Tg2576 mice (Ricobaraza et al. 2012).

The type of dietary fiber yields different SCFAs ratios: oligofructose (OF) and fructooligosaccharide (FOS) intake promotes a reduction in propionate but an increment in butyrate in rat cecum (Annison et al. 2003), whereas inulin (5 and 10%) increases all the three compounds compared to standard diets (Levrat et al. 1991). Fructans (F) from *Agave tequilana* promote acetate production in caecum, proximal-, medial-, and distal-colon and enhances butyrate levels in medial- and distal-colon, without changing propionate production, except in the distal-colon (Huazano-García and López 2013). Hence, we hypothesized that F intake would promote the abundance of butyrate-producing bacteria with concomitant butyrate production, preventing cognitive dysfunction in Tg mice. Therefore, we fed four-month-old male Tg mice with a control or an F-enriched diet for two months. Propionate levels were highly elevated in Tg-C mice, but F intake causes a reduction in the abundance of propionate-producing bacteria and propionate levels in fecal samples. F intake enhanced the survival of butyrate producers and butyrate concentration, decreasing astrocyte activation, and Aβ aggregation, preventing cognitive impairments in Tg mice. Antibiotic treatment reduced bacterial load and diversity, abating F´s cognitive improvements. Individual SCFAs evaluated in astrocyte cell culture showed propionate to promote glucose uptake and consumption, but butyrate exerted opposite effects. Hence, our data indicate that high-fiber intake promotes the survival of butyrate-producing bacteria and the production of butyrate with beneficial consequences for memory and learning abilities. Therefore, restoration of the propionate: butyrate ratio through modulation of GM by intake of soluble fiber can be considered a potential treatment against the onset of dementia and AD.

Materials and Methods

Experimental Design

Hemizygous Amyloid Precursor Protein/Presenilin 1 (APP/PS1: Tg) male mice (RRID: MMRRC-34832-JAX) expressing a chimeric mouse/human APP (Mo/HuAPP695swe) and a mutant human PS1 (PS1-dE9) transgenes on a C57BL/6 genetic background (Jackson Laboratory, Bar Harbor, ME, USA) and their wild-type (WT) littermates were used. All mice were housed individually with ad libitum access to food (Purina Rodent Chow 5001) and water under optimal vivarium conditions (12 h/12 h light–dark cycle, 20 ºC, and 40–50% relative humidity). Animal management and health status was supervised by licensed veterinarian care and approved by the Bioethics Committee of the Center for Research and Advanced Studies of the National Polytechnic Institute (Protocol No. 235–16), in accordance with the Mexican official standard NOM-062-ZOO-1999 and the principles set forth in the 8th edition of the National Institute of Health (NIH) guide for the care and use of laboratory animals and endorsed by the Institute for Laboratory Animal Research, the Division on Earth and Life studies and the National Research Council of the National Academies.

Dietary Protocol

Four months-old mice were exposed to a dietary protocol for 2 months with one of the following interventions:

- Control diet (C), prepared according to the American Institute of Nutrition (Reeves and Suppl 1997) with the following composition: Cornstarch (450.1 g/Kg), casein (140 g/Kg), maltodextrin (169.4 g/Kg), sucrose (100 g/Kg), soy oil (40 g/Kg), cellulose (50 g/Kg), mineral mix (35 g/Kg), vitamin mix (10 g/Kg), l-cysteine (3 g/Kg), choline (2.5 g/Kg), tertiary butylhydroquinone (TBHQ; 0.01 g/Kg). Energy: 3.90 kcal/g. A group of WT and Tg mice were fed with C diet ($n = 10$, each).
- 5% *Agave tequilana´*s derived fructans (F) (Bustar Alimentos, SA de CV) added to C diet with the following composition: Cornstarch (400.1 g/Kg), casein (140 g/Kg), maltodextrin (169.4 g/Kg), sucrose (100 g/Kg), soy oil (40 g/Kg), cellulose (50 g/Kg), mineral mix (35 g/Kg), vitamin mix (10 g/Kg), l-cysteine (3 g/Kg), choline (2.5 g/Kg), tertiary butylhydroquinone (TBHQ; 0.01 g/Kg), and *A. tequilana* fructans (50 g/Kg). Energy: 3.90 kcal/g. Tg mice were fed with F diet ($n = 10$).
- F diet plus antibiotic treatment (Abx) on drinking water (F-Abx). Antibiotic cocktail was prepared according to previous reports (Vikram et al. 2016): ampicillin [1 g/l], neomycin [1 g/l], metronidazole [1 g/l], and vancomycin [0.5 g/l], all dissolved in drinking water and given during four weeks before sacrifice. Tg-F mice were treated with Abx ($n = 10$).

Diets were designed to offer equal nutritional requirements and same caloric values (both, 3.90 kcal/g). They were administered in a dry form (5 g/day ad libitum, per animal) for 2 months. Body weight and food intake were monitored every two days. No significant differences in food intake and body weight change were seen during the course of the experiment (data not shown). No significant differences in the amount of drinking water were seen between antibiotics-treated mice and the other groups. However, bacterial load

(C_T) in cecum was lower in animals treated with antibiotics compared to the other groups indicating an appropriate efficacy of the antibiotic treatment (Fig. 4B).

Cognitive Assessment

One week before finalizing the dietary intervention, behavioral testing was performed. During habituation, animals were placed in the behavioral room two days before starting testing trials. Anxiety related behaviors were assessed by the Elevated Plus Maze (EPM). A 50 cm elevated plus-shaped maze made of medium-density fiberboard with a matte black acrylic surface and four arms (50 cm long × 10 cm wide), two without walls and two enclosed by 30 cm high walls, was used. The task consisted of 1 trial per animal, and only 1 choice phase where the animals were placed in the center facing an open arm. Entries into the open/close arms were recorded during 5 min and number of entries and percentage of time spent in the arms was calculated according to previous descriptions (Walf and Frye 2007). Recognition and working memory were evaluated by the Novel Object Recognition task (NOR) (Moojen et al. 2012). NOR test was carried out in a 40 × 40 cm open field with 40 cm high walls of plywood surrounding the floor. NOR task consisted of three phases as previously described (Moojen et al. 2012): (1) Habituation phase, animals were submitted to a habituation session where they explored the open field for 5 min without objects in the arena; (2) Training phase, 24 h after habituation, training trial was conducted by placing the rodents for 5 min in the arena from the same starting position and 2 objects of identical weight, size, texture, shape, and color positioned in 2 adjacent corners at 10 cm from the walls; (3) Trial phase, recognition memory test was carried out 1.5 h after the training phase by placing mice into the arena for 5 min in the presence of 1 familiar and 1 novel object (different weight, texture, shape, and color). A discrimination index (DI) was calculated as DI = (time with novel object − time with familiar object) / (time with novel object + time with familiar object). Between trials, all surfaces and objects were washed with 40% ethanol solution. Working memory was evaluated by the T-maze (TM). Briefly, a T-shaped maze apparatus of polymethylmethacrylate with starting arm (8.5 × 10.5 × 33.0 cm), and two choice arms (8.5 × 10.5 × 30.0 cm each, left and right) was used as previously described (Deacon and Rawlins 2006). TM task consisted of two phases. (1) Sample phase: animals were placed at the start arm and allowed to choose between left and right arms. A central divider was inserted into the start arm to create a start box. Once animals have chosen an arm, they were confined by plastic doors for 30 s. Thereafter, doors were re-opened, and mice were allowed to return to the start arm, where they were removed and returned to their home cages. (2) Choice phase: Two min later, animals were placed again in the start arm without the central divider and allowed to choose an arm. Animals were removed and placed in their home cages. Two hours later the procedure was repeated. At least three trials per day for 2 days were run for each animal. Percentage of alternations between arms was calculated. Finally, spatial memory was assessed by the Water Maze (WM). Briefly, WM task was carried out in a 100 cm diameter and 30 cm high round pool partially filled with 26 ºC white painted water as previously described (Nunez 2008). WM task consisted of three phases: (1) Training phase: mice were deposited from three different cardinal points and allowed to swim to reach a visible platform for 60 s; in case the animals did not find the platform during this time, they were gently guided and left in the platform for 20 s; (2) Learning phase: mice were allowed to swim in order to find a hidden platform in a maximum time of 60 s for 12 consecutive trials (in one-day), starting three non-consecutive times from each of the four different cardinal points; (3) Memory phase: After completion of the 12 trials, the platform was removed from the pool. Mice were released from the North-side and allowed to swim to find the missing platform in a maximum time of 30 s. The time spent to find the platform (latency) and the number of times the animal crosses the center of the pool (crossing quadrant) were recorded. All experiments were recorded with a Logitech DH Pro Webcam C920 camera connected to a computer equipped with Logitech Capture 1.10.110 and Eniima software (inhouse made software) to track animal's behavior and trajectory.

Tissue Preparation

One day after all behavioral trials were completed, mice were euthanized with pentobarbital sodium (150 mg/kg, i.p.) and cervical decapitation after retroorbital bleeding. Brains were immediately collected, and hemispheres were divided for further analysis. Right hemisphere was post fixed in 4% paraformaldehyde for 72 h at 4 ºC for immunohistochemistry (IHC) and immunofluorescence (IF) analysis. For IHC/IF, brain tissue was cryoprotected by immersion in 30% sucrose/water for three days. Coronal brain slices (40 µm thickness) were obtained with a sliding microtome (Leica Jung histoslide 2000 R). Sections from Bregma − 2.80 mm to − 2.92 mm (AP) were used for IHC, and from Bregma − 1.94 mm to − 2.18 mm (AP) for I*F* (Paxinos and Franklin 2001). All sections were immersed in cryoprotectant solutions, as previously described (Rodriguez-Callejas et al. 2016), and store at – 20 ºC until use.

Immunohistochemistry

Coronal sections were washed overnight in phosphate-buffered saline (PBS), incubated in 89% formic acid (Baker) for 15 min and then thoroughly washed with PBS. Sections were incubated in 0.3% H_2O_2 + 10% methanol in PBS for 30 min and then washed in 0.1% PBS-tween and incubated in 3% bovine serum albumin (BSA, Sigma) in 0.1% PBS-tween for 30 min. Thereafter, sections were incubated with Aβ antibody (BAM-10, 1:1000; Thermo Fisher Scientific Cat. No. MA1-91209) in 0.1% PBS-tween overnight at 4 ºC. After washing in 0.1% PBS-tween, sections were incubated with secondary antibody (1:500; Jackson ImmunoRes Cat. No. 115-035-146) in 1.5% horse serum diluted in 0.1% PBS-tween for 30 min at room temperature. Subsequently, sections were washed and incubated with the avidin–biotin complex (ABC Kit; Vector Laboratories) in 0.1% PBS-tween for 1.5 h according to the manufacturer's instructions. Finally, antibody binding was visualized with 0.025% 3,3′-diaminobenzidine (DAB Peroxidase Substrate Kit; Vector Laboratories) with 0.01% H_2O_2 as a catalytic agent. Sections were washed with PBS, dehydrated by serial dilution in ethanol and mounted in gelatin-coated slides with Eukit (Fluka). Control sections were processed without the primary antibody. Antibody has been validated in previous studies (Syeda et al. 2018).

Immunofluorescence

Brains sections were washed in PBS overnight and pre-treated with 1% sodium borohydride (Aldrich No. 19807-2) in distilled water at room temperature for 5 min. Then, tissue was washed with distilled water, returned to PBS for 5 min, and permeabilized with 0.5% PBS-tween for 6 min. Thereafter, sections were treated with blocking solution (50 mM glycine, 0.05% Tween20, 0.1% TritonX-100 and 0.1% BSA PBS-diluted) for 30 min at room temperature and incubated with primarly antibody (GFAP, 1:1000; Abcam Cat. No. Ab53554) diluted in antibody signal enhancer (ASE) solution (10 mM glycine, 0.05% Tween20, 0.1% TritonX-100, and 0.1% H_2O_2 PBS-diluted; according to Rosas-Arellano et al. 2016) during 48 h at 4 ºC. Then, slices were washed with 0.5% PBS-tween and incubated with the secondary antibody (1:500, Jackson ImmunoRes Cat. No. 705-605-147) and 1.5% donkey serum, all in 0.1% PBS-tween at room temperature for 2 h. Then, sections were washed with 0.5% PBS-tween and incubated with 4′,6-Diamidino-2-Phenylindole Dihydrochloride (DAPI; Invitrogen Cat. No. D1306) in 0.1% PBS-tween for 30 min, washed with 0.5% PBS-tween, and mounted on glass slides. Slices were cover slipped with mounting medium (Vecta shield, Vector Laboratories). Control sections were processed without the primary antibody. Antibody has been validated in previous studies (Syeda et al. 2018).

Image Acquisition and Analysis

To detect Aβ aggregates, brightfield images were obtained by a Nikon Eclipse 80i light microscope equipped with a Nikon DS-Ri1 camera. All images were taken at same light exposure. Tissue background staining was subtracted from optical density values and threshold was determined by identifying best signal-to-noise ratio using the wand tool in legacy mode (Leica Application Suite X). Number and area of Aβ aggregates ≥ 100 μm^2 were determined using the Fiji v. 1.46 (NIH, open access) plugin "measure" in hippocampus, cortex (visual and auditory cortices) and layers I–VI from entorhinal cortex in pixels-to-μm scaled ×10 images.

Images of GFAP + astrocytes were obtained by a confocal microscope (Leica TCSSP8) with argon (488 nm), and helium/neon (543 nm) lasers. Both lasers were always used with optimized pinhole diameter. Stacks were super imposed as a single image with Leica Application Suite X Life Science Microscope Software. A maximum projection was obtained in a two-dimensional plane. GFAP + astrocytes were quantified using the Fiji v. 1.46 plugin "analyze particles" in dentate gyrus, *stratum* (*st.*) *radiatum* and *st. oriens* of CA1 hippocampal region, and layers I–VI from entorhinal cortex, all using a ×40 objective. In order to quantify astrocytic processes length and branching points, Sholl analysis was carried out as follow: GFAP + astrocytes located in *st. radiatum* were imaged with a ×63 immersion objective performing optimized optical scanning in Z axis and processed by the tool "build neurites n" (NeuronStudio Software 0.9.92 by Computational Neurobiology and Imaging Center of the Icahn School of Medicine at Mount Sinai; Binley et al. 2014). We have chosen *st. radiatum* due to previous regional alterations reported in Tg mice (Perez-Cruz et al. 2011; Syeda et al. 2018).

Fecal Microbiota Analysis

Fecal samples were collected for each animal one week before sacrifice. Animals were placed for 1 h in a Super Mouse 750™ Micro-Isolator® system cage (15 cm width × 30 cm long × 17 cm high) previously cleaned and disinfected. At least 100 mg of feces pellets were collected per animal, immediately frozen and store at − 70 ºC until use. Bacterial DNA was extracted using the FavorPrep™ Stool DNA Isolation Mini Kit (Favorgen Biotech Corp, Cat. No: FASTI001-1) according to the manufacturer´s instructions. The purified DNA quantity was measured using 260/280 nm absorbance using a Nano Drop 2000 spectrophotometer (Thermo Scientific), and its quality was

evaluated by 0.5% agarose gels electrophoresis. Genomic libraries of ~ 281 base pairs (bp) 16S rDNA 3rd hypervariable region (V3) amplicons were generated for each experimental subject using specific V3-341F primers against V3 that also contained a different 12-bp Golay barcode (set of barcodes 1–100) complementary to position 340–356 of *Escherichia coli* 16S rRNA molecule *rrnB* GeneBank J01859.1 and an overhang adapter specified by Ion Torrent, and V3-518R reverse primers complementary to position 517–533 of the same molecule (Corona-Cervantes et al. 2020). The amplicons of the V3 regions were generated by 1X 50 µl polymerase chain reactions (PCR) containing 1 µl of 10 µM forward primer, 1 µl of 10 µM reverse primer (settings specified above), 0.25 µl of 5U/µl high thermostable DNA recombinant polymerase (Thermo Scientific No. EP0402), 1 µl of 10 mM dNTP mix (Thermo Scientific No. R0191), 4 µl of 25 mM $MgCl_2$ (Thermo Scientific No. R0971), 5 µl of 10X taq buffer with KCl (100 mM Tris–HCl [pH 8.8 at 25 °C], 500 mM KCl, and 0.8% volume/volume [% v/v] nonidet P40, Thermo Scientific No. B38), and 20 ng of genomic DNA in 37.75 µl of nuclease-free water (Thermo Scientific No. R0581) per reaction. Amplification was carried out using Applied Biosystem Veriti Thermal Cycler (amplification conditions are shown in Table S1). For sequencing, equivalent amounts of 1 to 100 barcoded amplicons (10 µg each) were combined. Each mix was purified using E-Gel iBase Power System (Invitrogen). The libraries size and concentration were determined using an Agilent 2100 Bioanalyzer, and libraries for each run were diluted to 26 pM prior to clonal amplification. Emulsion PCR was carried out using the Ion OneTouch™ 200 Template Kit v2 DL (Life Technologies), according to the manufacturer´s instructions. Amplicon enrichment with ion spheres was done using Ion OneTouch ES. The sequencing was done using the Ion 316 Chip Kit v2 and the Ion Torrent Personal Genome Machine (PGM) System. After sequencing, reads were filtered by the PGM software to remove low quality and polyclonal sequences. During this process, sequences matching the 3' adapters were automatically trimmed and filtered. Ion Torrent PGM software, Torrent Suite v4.0.2, was used to demultiplex the sequenced data based on their barcodes. Poor quality reads were eliminated from the datasets, i.e., quality score ≤ 20, containing homopolymers > 6, length < 200 nucleotides (nt), and containing errors in primers or barcodes. Filtered data were exported as FASTQ files. Demultiplexed sequencing data were analyzed using quantitative insights into microbial ecology (QIIME) software v1.9.0 pipeline (Caporaso et al. 2010). FASTQ files were converted into FASTA files, and all demultiplexed files were concatenated into a single file. Closed reference OTUs were determined at the 97% similarity level using the UCLUST algorithm. Chimeras were detected and removed from the datasets using the ChimeraSlayer. Sequence alignments were done against the Greengenes 13.9 core set (sequencing summary is shown in Table S2). *Taxa* richness measurements (Observed and Chao1) and alpha diversity indexes (Shannon and Simpson) were calculated. Weighted and unweighted UniFrac distances were used to perform the principal coordinate analysis (PCoA). Microbial sequence data were pooled for OTUs comparison and taxonomic abundance analysis but separated by batch in PCoA to have clear PCoA figures using Emperor. Community diversity was determined by the number of OTUs and beta diversity, measured by UniFrac unweighted and weighted distance matrices in QIIME software v1.9.0. Analysis of similarities (ANOSIM) and permutational multivariate analysis of variance (ADONIS), permutational multivariate analysis of variance using distance matrices methods were used to determine statistically significant clustering of groups based upon microbiota structure distances. Furthermore, linear discriminant analysis (LDA) effect size (LefSe) program v1.0 was used to perform LDA (scores ≥ 2) to estimate significant effect size of each bacterial *taxa* between experimental groups (Segata et al. 2011).

Metagenome Prediction

We used Phylogenetics Investigation of Communities by Reconstruction of Unobserved States (PICRUSt v.1.1.1) to predict related metabolic profiles of the metagenomes from 16S rDNA gene data set by Kyoto Encyclopedia of Genes and Genomes (KEGG) orthologs classification database at hierarchy level 3 pathways. Statistical Analysis of Taxonomic and Function (STAMP v2.1.3) software was used to determinate significant differences in abundance of OTUs related to metabolic pathways (Langille et al. 2013).

Short Chain Fatty Acids Concentration

SCFA content in fecal samples was analyzed by high performance liquid chromatography (HPLC; PerkinElmer Series N3896). The collected fecal samples were dried to constant weight and subsequently processed using the solid-phase extraction (SPE) method (Agilent Technologies 1260). At least 50 mg of dried feces were suspended completely in 1 ml of deionized water by vigorous mixing in a vortex at maximum speed for 10 min. The suspension was centrifuged at 13,000 rpm for 10 min, the supernatant was transferred to a fresh tube and passed through activated C-18 max 100 mg/ml GracePure™ Reversed-Phase SPE Columns according to the manufacturer's instructions. SCFAs were eluted with 1 mL of filtered water (Nylon Syr Filter, 13 mm, 0.22 µm) and analyzed via HPLC using 20:80 acetonitrile: NaH_2PO_4 (pH 2.2 using phosphoric acid, Sigma-Aldrich No. S8282-500G) as mobile phase (De Baere et al. 2013). Standard curves were prepared for acetate

(Sigma-Aldrich No. 45754-100ML-F), propionate (Sigma-Aldrich No. P1386-500ML), and butyrate (Sigma-Aldrich No. B103500-500ML).

Morphology of the Intestinal Layers

We collected the proximal-colon and performed hematoxylin/eosin staining as previously described (Piedra-Quintero et al. 2019). Briefly, the tissue was washed in PBS 1X, fixed with 4% paraformaldehyde, and embedded in paraffin. Five µm cross-sections were mounted on glass slides and used for hematoxylin/eosin (H&E) Masson's Trichrome standard protocol staining (Medina-Buelvas et al. 2019). Histological examinations were performed by light microscopy (Fernández-Martínez et al. 2018) and images were analyzed by Fiji software v1.46.

Lipopolysaccharide Levels in Plasma

Plasma samples were processed for lipopolysaccharide (LPS) quantification using an enzyme-linked immunosorbent assay (ELISA; Cloud-Clone Corp, USA) kit according to the manufactures' instructions (Sánchez-Tapia et al. 2017).

In Vitro Studies

Genetically Encoded Förster Resonance Energy Transfer (FRET) Sensors

We used the FRET sensor FLII12Pglu700mΔ6 (Addgene 17866) for live intracellular glucose measurement in astrocytes (Takanaga et al. 2008). Briefly, mixed F1 male mice (C57BL/6J) were used to obtain cortical cultures of neuronal and glial cells (from P1 to P3 neonatal mice). Cultures were maintained at 37 °C in a humidified atmosphere of 5% CO_2. Seven days-old cell culture was infected with FLII12Pglu700mΔ6 overnight. Cells were transduced with adeno-associated virus (AAV9) expressing FLII12Pglu700µΔ6 under the control of the GFAP (short gfaABC1D) promoter. Next morning medium was changed, and the culture was treated with different concentration of propionate (0.25 mM, 0.5 mM, and 2 mM), butyrate (0.125 mM and 2 mM) for three days. On day 11 fluorescence imaging was done with an Olympus IX70 or BX51 microscopes equipped with Optosplits and a Hamamatsu Orca camera. Cells were superfused at room temperature with a 95% air and 5% CO2-gassed solution of the following composition (mM): 112 NaCl, 3 KCl, 1.25 $CaCl_2$, 1.25 $MgCl_2$, 2 glucose, 1 Na-lactate, 10 HEPES and 24 $NaHCO_3$, pH 7.4 (Valdebenito et al. 2016). During imaging, astrocytes were exposed to zero glucose (no glucose on the medium), Cytochalasin B (Sigma-Aldrich, 20 µM), and Azide (Sigma-Aldrich, 5 mM) solutions. We recorded changes in fluorescence intensity on exposure to these stimuli. Fluorescence was then converted to glucose concentration. The Citrine channel was divided by the CFP channel and the ratio (R) subtracted from average values of zero glucose to get ΔR and glucose concentration was obtained with the formula (-0.43*ΔR)/(ΔR -0.6). All experiments were approved by the animal Care and Use Committee of Centro de Estudios Científicos, Chile.

Bioenergetic Analysis in Cultured Astrocytes

Primary cortical astrocyte culture was used through a method previously described by Escudero-Lourdes et al. 2016, modified for the mouse brain. P0-P1 C57BL/6 mouse brain cortices were dissected manually in Hank´s Balanced Salt Solution (HBSS; Thermo Scientific No. 14025076) tempered to 37 °C. Astrocytes were grown at 37 °C and 5% CO_2 in high glucose Dulbecco's Modified Eagle Medium (DMEM; Thermo Scientific No. 11965118) supplemented with 10% fetal bovine serum (FBS) and 1% penicillin/streptomycin. Then, 2×10^4 astrocytes/well were seeded at in a Seahorse Extracellular Flux (XF) 96 Analyzer (Agilent Technologies) in cell culture microplates (Agilent Technologies No. 101085-004) pre-treated for 1 h with 4 °C poly-D-lysine (PDL; Thermo Scientific No. A3890401), and grown until they reached 70% to 80% confluence and treated for 2 or 72 h with DMEM (control) or 0.5 and 1 mM of acetate (Sigma-Aldrich No. 45754-100ML-F), propionate (Sigma-Aldrich No. P1386-500ML) or butyrate (Sigma-Aldrich No. B103500-500ML), all diluted in DMEM (De Almeida et al. 2006).

Oxygen consumption rate (OCR) and extracellular acidification rate (ECAR) was assessed under a Seahorse analyzer as described by Ovalle-Magallanes et al. 2019. Briefly, cultured astrocytes were washed with XF base medium supplemented with glucose (Sigma-Aldrich 25 mM), glutamine (Sigma-Aldrich 1 mM), and pyruvate (Sigma-Aldrich 1 mM, pH 7.4), and then incubated in this medium for 1 h at 37 ºC in a non-CO_2 incubator. The plates were placed in the Seahorse analyzer at 37 ºC for a 10 min calibration time, and three measurement cycles were run to record basal cellular respiration. Oligomycin (Sigma-Aldrich, 4 µM), carbonyl cyanide-4-(trifluoromethoxy) phenylhydrazone (Sigma-Aldrich, FCCP; 1 µM), and a mixture of rotenone and antimycin A (Sigma-Aldrich,1 µM) were sequentially added. Six measurements were performed after treatment with acetate (Sigma-Aldrich 0.5 and 1 mM), propionate (Sigma-Aldrich 0.5 and 1 mM), and butyrate (Sigma-Aldrich 0.5 and 1 mM) either during 2 or 72 h incubation period. Basal respiration was calculated as the average OCR at initial conditions, as a parameter to estimate the respiration used to meet the endogenous adenosine triphosphate (ATP) demand of the cell and drive proton leak pathways; ATP-linked respiration with the

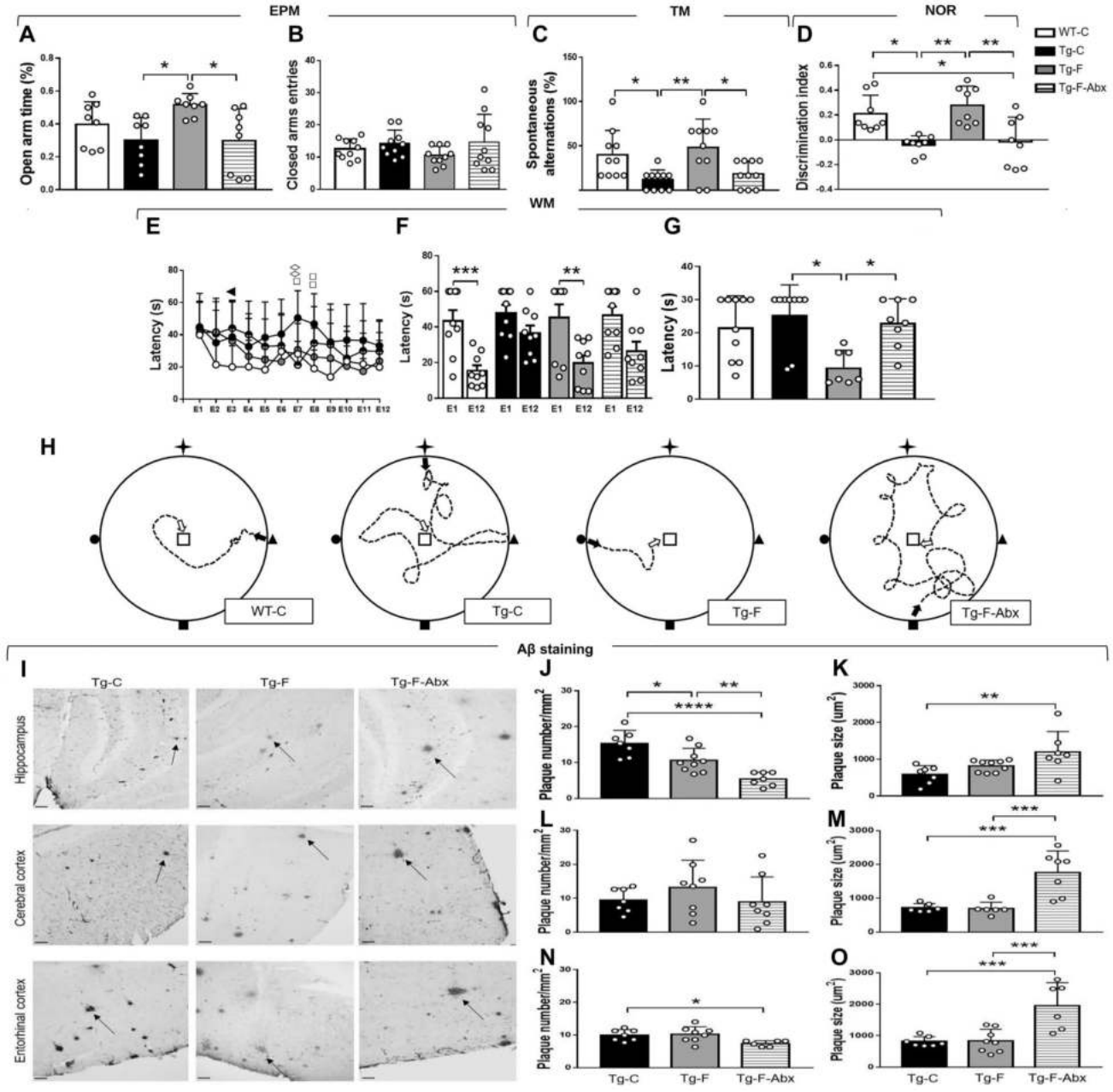

difference between the average basal OCR and the average OCR obtained after addition of oligomycin as a parameter to estimate the respiration that is sensitive to oligomycin and used to drive mitochondrial ATP synthesis; proton leak with the difference between the average OCR obtained after addition of oligomycin and the average minimum OCR as a parameter to estimate the incomplete coupling of oxidative phosphorylation due to the leak of protons across the inner membrane independently of ATP synthesis; maximal respiration as the difference between the average OCR obtained after addition of FCCP and the average OCR obtained after addition of rotenone and antimycin A mixture as a parameter to estimate the maximum rate of respiration; spare respiratory capacity with the difference between the average basal OCR and the average OCR obtained after addition of FCCP, as a parameter to estimate the amount of extra ATP that can be produced by oxidative phosphorylation in case of a sudden increase in energy demand; and non-mitochondrial respiration with the average minimum OCR as a parameter to estimate the OCR-dependent respiration after blocking mitochondrial oxidative phosphorylation upon addition of electron transport chain inhibitors such as rotenone and antimycin A (Divakaruni et al. 2014). For ECAR measurements, oligomycin, FCCP, and the mixture of rotenone and antimycin A sequentially added for mitochondrial respiration protocol; 2-deoxyglucose (Sigma-Aldrich, 2-DG) was added

◂**Fig. 1** Effect of fructans intake in anxiety, learning, and memory. Antibiotic treatment reduces amyloid-β aggregation in the brain. **A** Anxiety was inversely proportional to the time spent in the open arm [F (3, 28) = 4.214], and **B** directly proportional to the time spent in the closed arms [F (3, 36) = 1.263] in the EPM. **C** Working memory was directly proportional to the spontaneous alternations [F (3, 36) = 5.741] in the T-maze. **D** Recognition memory was directly proportional to the discrimination index [F (3, 28) = 9.007] in the NOR test. **E** Spatial learning curve was inversely proportional to the latency to find the hidden platform [F (11, 432) = 2.52] in the WM. X axis corresponds to the 12 consecutive learning trials. **F** Learning performance was compared between trial No.1 and trial No.12 [F (7, 64) = 6.209]. **G** Spatial memory was inversely proportional to the latency to find the place where the platform was located after trainings [F (3, 30) = 5.608]. **H** Representative schemes of mice trajectory (dotted line and white arrow) from the start point (black arrow) to the platform area (central square) in the WM test. Cardinal points are marked in maze walls as a star-shaped polygon (north), a square (south), a triangle (west) and a circle (east). **I** Representative images of Aβ plaques in the hippocampus, Cx and ENT for Tg-C, Tg-F, and Tg-F-Abx mice. Amyloid plaques are pointed by black arrows. Scale bar equals 100 µm. **J** Quantification of Aβ plaques [F (2, 20) = 17.75] and **K** relative plaque size F (2, 20) = 5.61] in hippocampus. **L** Quantification of Aβ plaques [F (2, 20) = 0.95] and **M** relative plaque size [F (2, 16) = 14.52] in Cx. **N** Quantification of Aβ plaques [F (2, 18) = 4.63] and **O** relative plaque size [F (2, 18) = 12.59] in ENT. For A, WT-C n = 9, Tg-C n = 9, Tg-F n = 9, and Tg-F-Abx n = 9. For B-H, WT-C n = 10, Tg-C n = 10, Tg-F n = 10, and Tg-F-Abx n = 10. For K-P, Tg-C n = 4, Tg-F n = 4, and Tg-F-Abx n = 4. For all white color circles within bars indicate experimental subjects, except E, where circles indicate experimental groups. Data are shown as mean ± SD bars. Data between square brackets indicate F (DFn, DFd) values of one-way ANOVA with Tukey post hoc correction. For **A**–**D**, **F**, **G**–**H**, and **K**–**O**, one-way ANOVA with Tukey post hoc correction; *p < 0.05, **p < 0.01, ***p < 0.001, and ****p < 0.0001. For **E**, two-way ANOVA with Tukey post hoc correction; statistical significance between WT-C versus Tg-C is shown by □ symbol, WT-C versus Tg-F by ■, WT-C versus Tg-F-Abx by Δ, Tg-C versus Tg-F by ▲, Tg-C versus Tg-F-Abx by ◊, and Tg-F versus Tg-F-Abx by ◆; one symbol p < 0.05, two symbols p < 0.01

and three measurements were performed. We calculated glycolytic capacity as the difference between the average ECAR obtained after addition of oligomycin and the average ECAR obtained after addition of 2-DG, estimating the maximum rate of conversion of glucose to pyruvate or lactate (Mookerjee et al. 2016); glycolytic reserve was calculated as the difference between the average basal ECAR and the average ECAR obtained after addition of oligomycin, as a parameter to estimate the difference between glycolytic capacity and glycolytic rate (Das 2013).

Statistical Analysis

Data are expressed as the mean ± standard deviation (SD). Differences between experimental groups were compared by one-way analysis of variance (ANOVA) followed by Tukey´s range test, except for the behavior learning curves, Sholl analysis, OCR, and ECAR, that were analyzed by a two-way repeated measure ANOVA followed by Tukey´s range test. Differences for *taxa* enrichment and abundance of sequences related to metabolic pathways were evidenced by LefSe and ANOVA followed by Tukey–Kramer post hoc test, respectively. β diversity was analyzed by ANOSIM and ADONIS. All results were considered statistically significant at $p < 0.05$.

Results

Soluble Fiber Intake Prevents Anxiety and Memory Impairments in Tg Mice

We evaluated anxiety in six-month-old mice. No significant differences were seen between WT-C and Tg-C mice, but Tg-F mice spent more time in the open arms than Tg-C mice, indicating an anxiolytic effect. Antibiotic-treated Tg-F mice lost this anxiolytic effect (Fig. 1A, B).

Short-term working memory, recognition, and spatial memory were evaluated by the T-maze test (TM), the novel object recognition test (NOR), and the water-maze test (WM), respectively. In TM, Tg-C mice showed a lower percentage of spontaneous alternations than the WT-C group, but an improved working memory was observed in Tg-F mice. Notably, antibiotic treatment abolished this cognitive improvement (Fig. 1C). In NOR, recognition memory impairment was seen in Tg-C mice compared to WT-C, a condition prevented by F intake; however, DI was reduced in antibiotic-treated mice (Tg-F-Abx mice, Fig. 1D). In the WM, we observed effective spatial learning in WT-C and Tg-F mice, as latencies to find the platform was shorter in trial 12 (E12) compared to trial 1 (E1). However, Tg-C and Tg-F-Abx mice had similar latencies in E1 and E12, indicating impaired learning (Fig. 1E, F). Spatial memory was also improved in Tg-F mice than in Tg-C and Tg-F-Abx mice (Fig. 1G). Thus, a two-month F intake prevented hippocampal and cortical-related cognitive impairments in Tg mice.

Increased Aβ load during aging is associated with memory impairments (Lim et al. 2014). As we observed a preserved cognitive function in Tg-F mice, we evaluated whether this neuroprotective effect may be related to brain Aβ aggregation.

Antibiotic Treatment Reduces Brain Amyloid-β Aggregation

We analyzed the number and the size of Aβ plaques in the hippocampus, cerebral, and entorhinal cortices (Fig. 1I–O). A reduction in the number of Aβ plaques in the hippocampus was seen in Tg-F mice compared to Tg-C mice. Notably, antibiotic treatment had a major impact on Aβ aggregation in the hippocampus, as it caused a drastic reduction in the number of Aβ plaques compared to the Tg-C and Tg-F

groups (Fig. 1J). In the cortex, no differences in the number of Aβ plaques were observed among groups (Fig. 1L). In the entorhinal cortex, antibiotic treatment reduced the number of Aβ plaques compared to Tg-C (Fig. 1N). As we noticed a more diffused Aβ aggregation in Tg-F mice than in the other groups, we determined the size of the plaques in each brain region. We observed that antibiotic treatment caused an enlarged plaque size compared to the Tg-C group in the hippocampus and cortices compared to Tg-C and Tg-F mice (Fig. 1K, M, and O). Previous studies have reported an anti-amyloid effect of antibiotic treatment (Minter et al. 2017). Notwithstanding a substantial reduction in the number and the increased size of Aβ plaques, no improvements in cognitive functions were seen in in Tg-F-Abx mice (Fig. 1A–H). In contrast, despite a mild effect in the number of Aβ plaques in the hippocampus of Tg-F mice, a substantial recovery in the spatial- and short-term memorie were seen in these mice, with scores similar to the WT-C group.

In the early stages of AD, there is an increased number of reactive astrocytes (González-Reyes et al. 2017; Li et al. 2011), and astrocytic metabolic alterations are proposed as triggering factors for cognitive impairment (Le Douce et al. 2020; Kashon et al. 2004). Therefore, we explored the impact of F intake on astrocyte activation.

Soluble Fiber Intake Effectively Decreased Hippocampal Astrogliosis in Tg Mice

We determined the number of GFAP + astrocytes in the hippocampus (dentate gyrus, *st. radiatum*, *st. oriens*) and entorhinal cortex from WT-C, Tg-C, Tg-F, and Tg-F-Abx mice (Fig. 2). An increased number of GFAP + astrocytes in the dentate gyrus, *st. radiatum* and *st.oriens* were observed in Tg-C mice compared to WT-C mice (Fig. 2B–D). A normalization in the number of GFAP+ astrocytes to control values was seen in Tg-F mice in dentate gyrus and *st. radiatum* (Fig. 2B, C). In *st. radiatum*, Tg-F-Abx mice showed a fewer number of astrocytes compared to Tg-C mice (Fig. 2C). No significant differences between groups were seen in the entorhinal cortex (Fig. 2E). An elongation of astrocytic processes is an indicator of cellular reactivity (Rose et al. 2020). To determine whether the enhanced number of GFAP+ astrocytes was associated with a reactive phenotype, we determined their processes morphology by a Sholl analysis. We evaluated astrocytes located in the *st. radiatum* (three cells per animal and four animals per group) (Fig. 2F–I). We selected *st. radiautum* as it showed the most prominent alterations in Tg-C mice compared to the other brain regions analyzed. A significant difference in process length (8 to 22 µm from the soma) was observed in Tg-C mice compared to the other groups (Fig. 2F, G). The dendritic length and total number of branching points were increased in Tg-C mice compared to WT-C. Tg-F and Tg-F-Abx mice showed a reduction in process length and branching points (Fig. 2G, H). We then hypothesized that fermented bacterial products (i.e., SCFAs) might be implicated in F´s neuroprotective effect as they modulate astrocyte metabolism and reactivity. SCFAs and other bacterial bioproducts, such as lipopolysaccharide (LPS), can translocate from the intestine to blood circulation when the gut epithelium is disrupted. Then, we analyzed the gut integrity and determined the concentration of SCFAs and LPS levels in fecal and plasma samples, respectively.

Intestinal Morphological Alterations and Lipopolysaccharide Plasma Levels are Reduced in Mice Treated with Soluble Fiber, an Effect Associated with Restoring Butyrate and Propionate Production

Intestinal morphology alterations were seen in Tg-C and Tg-F-Abx mice, with atrophied and aberrant shapes in cilia and goblet cells (Erben et al. 2014) compared to WT-C and Tg-F animals (Fig. 3A); this was further reflected by a thinner submucosa layer in Tg-C and Tg-F-Abx mice compared to WT-C and Tg-F mice (Fig. 3B). No changes in the muscular layer thickness were seen among groups (Fig. 3C). Damage to the gut epithelial barrier was accompanied by augmented LPS plasma levels in Tg-F-Abx mice compared to WT-C and Tg-F groups (Fig. 3D).

The fecal concentration of acetate, propionate, and butyrate was also measured. Acetate concentration achieved WT-C values in Tg-F mice, higher than in Tg-C and Tg-F-Abx mice (Fig. 3E). Propionate concentration was the highest in Tg-C mice compared to other groups (Fig. 3F). Contrary, butyrate concentration was the highest in Tg-F mice, but antibiotic treatment abolished these increments (Fig. 3G).

As we noticed important increments in butyrate concentration after F intake and Tg-F mice showed better cognitive performance, we ran association analysis between specific readouts to determine the possible association with astrocyte activation, Aβ plaques numbers, and cognitive performance. We used data only from animals from which we could associate two or more parameters. Butyrate concentration negatively correlated with the number of reactive astrocytes in the hippocampus (Fig. 3H) but had a positive correlation with the discrimination index (DI) in the recognition memory test (Fig. 3K). Contrary, propionate concentration positively correlates with the number of reactive astrocytes in the hippocampus (Fig. 3I) and with the number of Aβ plaques (Fig. 3L). LPS plasma levels were the highest in the Tg-F-Abx group, and correlation analysis showed LPS to be negatively correlated with the total number of Aβ plaques (Fig. 3J) but negative correlated with DI (Fig. 3M). This data indicates that F-intake favors butyrate production instead of

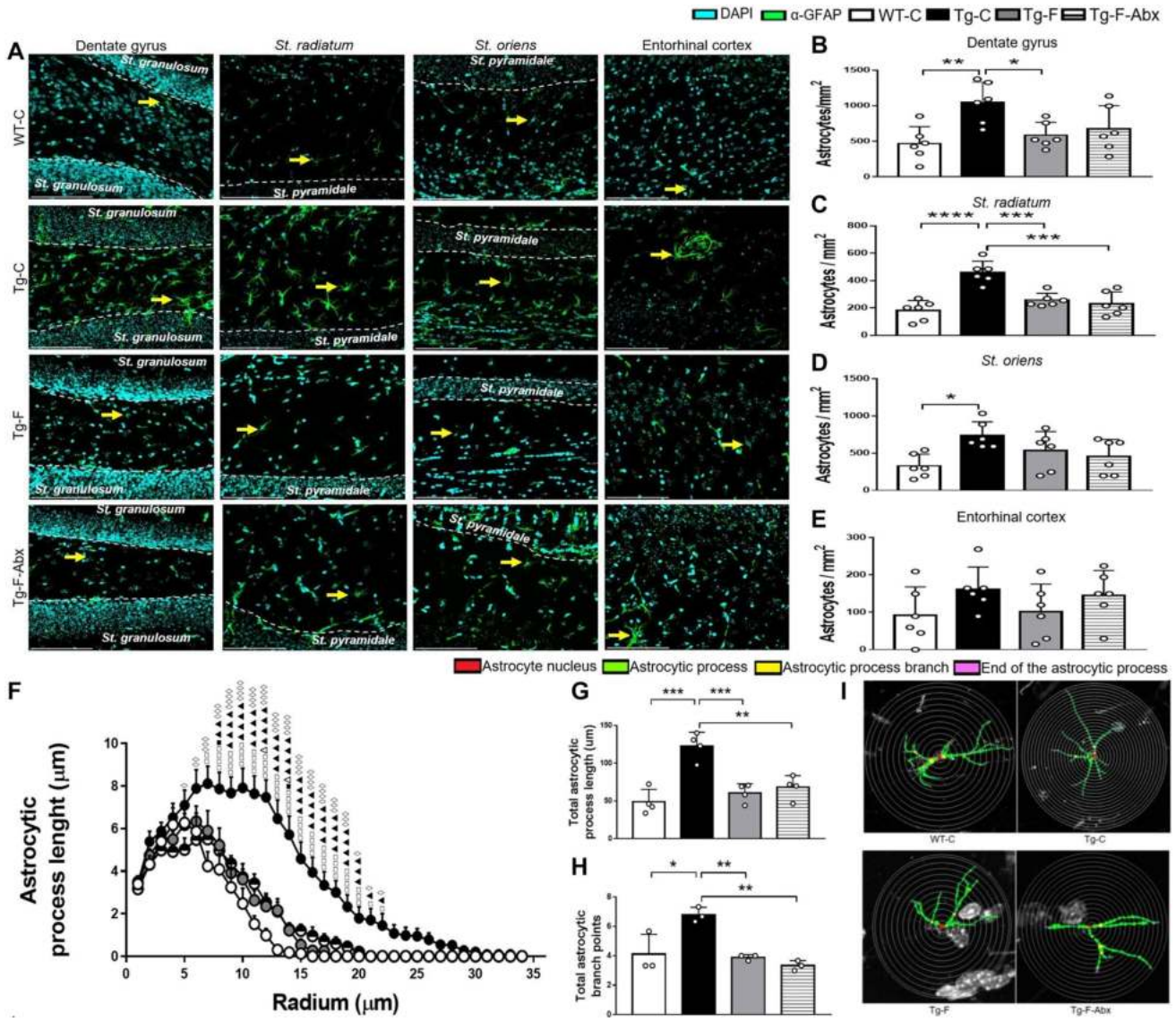

Fig. 2 Evaluation of neuroinflammation. **A** Representative images of GFAP-positive astrocytes in the dentate gyrus, st. radiatum, st. oriens, and ENT of WT-C, Tg-C, Tg-F, and Tg-F-Abx mice. GFAP-positive astrocytes are pointed by yellow arrows. Scale bar 100 µm. **B** GFAP-positive astrocytes per mm2 F [(3, 20) = 5.266] in dentate gyrus. **C** GFAP-positive astrocytes per mm2 [F (3, 20) = 16.35] in st. radiatum. **D** GFAP-positive astrocytes per mm2 [F (3, 20) = 4.033] in st. oriens. **E** GFAP-positive astrocytes per mm2 [F (3, 20) = 1.393] in ENT. (**F**Sholl analysis of astrocytic processes length (µm) from all groups, with a range distance of 1 µm between consecutive circumferences [F (33, 1496) = 112.5]. **G** Total astrocytic processes length [F (3, 12) = 17.3]. **H** Total astrocytic branch points [F (3, 8) = 12.73]. **I** Representative images of GFAP-positive cells used form the Sholl analysis. For B-E, WT-C $n = 4$, Tg-C $n = 4$, Tg-F $n = 4$, and Tg-F-Abx $n = 4$. For F-G, WT-C $n = 4$, Tg-C $n = 4$, Tg-F $n = 4$, and Tg-F-Abx $n = 4$. For H, WT-C $n = 3$, Tg-C $n = 3$, Tg-F $n = 3$, and Tg-F-Abx $n = 3$. White circles within bars indicate each experimental subject. For B-E and G-H, one-way ANOVA with Tukey post hoc correction; $*p < 0.05$, $**p < 0.01$, $***p < 0.001$, and $****p < 0.0001$. For F, two-way ANOVA with Tukey post hoc correction; statistical significance between WT-C versus Tg-C is shown by □ symbol, WT-C versus Tg-F by ■, WT-C versus Tg-F-Abx by Δ, Tg-C versus Tg-F by ▲, Tg-C versus Tg-F-Abx by ◊, and Tg-F versus Tg-F-Abx by ♦; one symbol represents $p < 0.05$, two symbols $p < 0.01$, three symbols $p < 0.001$, and four symbols $p < 0.0001$; circles indicate experimental groups. Data are shown as mean ± SD bars. Data between square brackets indicate F (DFn, DFd) values of one-way ANOVA with Tukey post hoc correction

propionate in Tg mice. Restoration of butyrate: propionate ratio in Tg-F mice was associated with an improved cognitive performance. Notably, propionate in Tg-F-Abx mice did not return to Tg-C levels; it remained low. This low propionate concentration in antibiotic-treated mice may explain the reduced number of reactive astrocytes in Tg-F-Abx mice, due to the neurotoxic properties of propionate. Despite the absence of propionate and the reduced number of reactive astrocytes in Tg-F-Abx, the fiber diet´s cognitive protection was lost (Fig. 1). Hence, F´s neuroprotective effects could

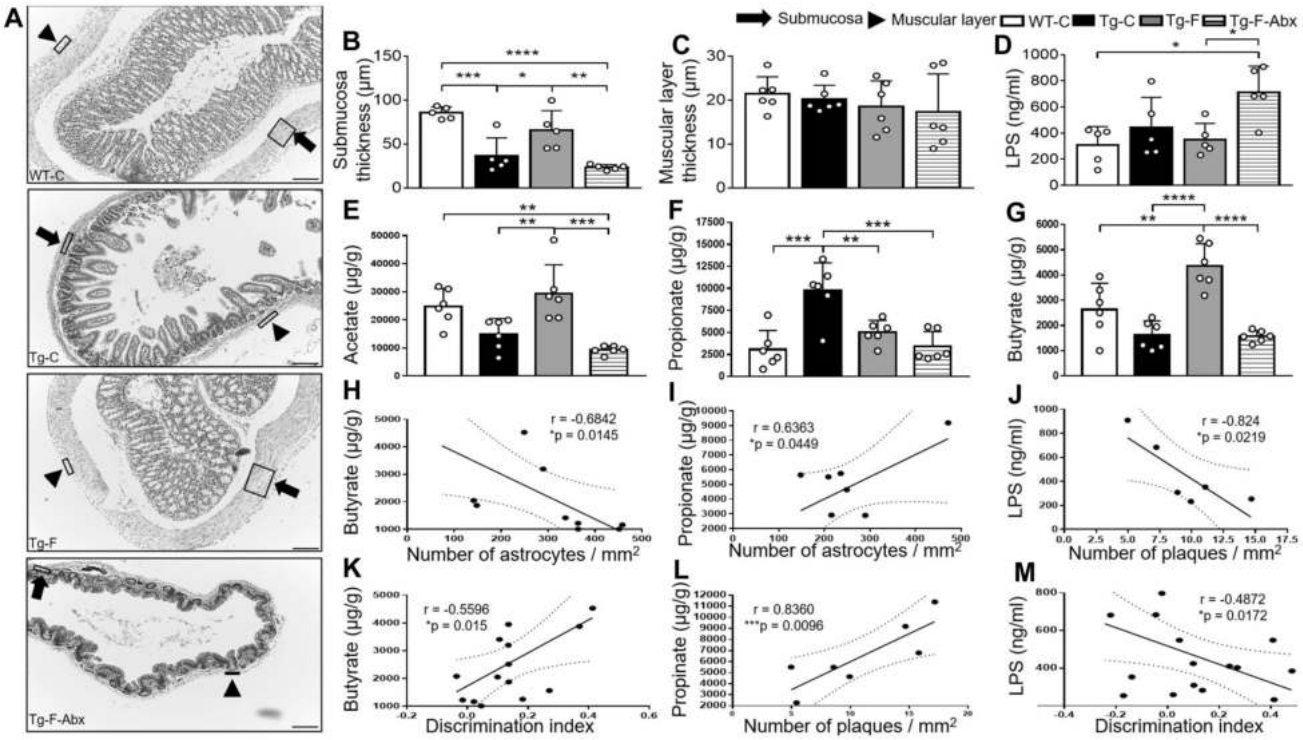

Fig. 3 Gut integrity, LPS plasma levels and SCFAs concentration in feces. **A** Representative images of cross-sectional gut slices of WT-C, Tg-C, Tg-F, and Tg-F-Abx mice. Scale bar 100 µm. **B** Submucosa thickness [F (3, 8) = 5.28] for experimental groups. **C** Muscular layer thickness [F (3, 8) = 0.28] for experimental groups. **D** LPS plasma concentration [F (3, 16) = 5.022]. **E** Acetate concentration [F (3, 20) = 11.3] in feces. **F** Propionate concentration [F (3, 20) = 12.01] in feces. **G** Butyrate concentration [F (3, 20) = 18.22] in feces. White color circles within bars indicate experimental subjects. For **B**–**G**, one-way ANOVA with Tukey post hoc correction; data are shown as mean $n \pm$ SD bars; $*p < 0.05$, $**p < 0.01$, $***p < 0.001$, and $****p < 0.0001$. Data between square brackets indicate F (DFn, DFd) values of one-way ANOVA with Tukey post hoc correction. Butyrate concentration had a negative correlation with the number of reactive astrocytes (**H**), but a propionate had a positive correlation (**I**). LPS plasma levels showed a negative correlation with number of plaques (**J**), but propionate showed a positive association (**L**). Butyrate concentration showed a positive correlation with the recognition memory (**K**), but LPS showed a negative correlation (**M**). For all correlations, statistical analyses were performed using the Spearman's test ($p < 0.05$ as significance set). For **A**, **C**, and **E**–**G**, $n = 6$ for each experimental group; for **B** and **D**, $n = 5$ for each experimental group; For **H**, WT-C $n = 2$, Tg-C $n = 3$, Tg-F $n = 3$, and Tg-F-Abx $n = 2$; For **I**, WT-C $n = 2$, Tg-C $n = 2$, Tg-F $n = 2$, and Tg-F-Abx $n = 2$; For **J**, Tg-C $n = 2$, Tg-F $n = 2$, and Tg-F-Abx $n = 2$; For **K**, WT-C $n = 6$, Tg-C $n = 3$, Tg-F $n = 3$, and Tg-F-Abx $n = 3$; For **L**, Tg-C $n = 2$, Tg-F $n = 3$, and Tg-F-Abx $n = 2$. For **M**, WT-C $n = 6$, Tg-C $n = 3$, Tg-F $n = 4$, and Tg-F-Abx $n = 3$

be attributed to the enhanced butyrate production. To determine what bacteria taxa is being modulated by the high-fiber diet, we collected fecal samples at the end of the treatments, and determined the relative abundances of all sequenced gut bacteria.

Soluble Fiber Ingestion Decreased the Abundance of Propionate-Producing Bacteria but Increased that of Butyrate-Producers

We noticed several differences between groups at the phylum (P) level. Tg-C mice had a higher abundance of Firmicutes than WT-C (81.3% *vs*. 75.8%, respectively), but it was significantly reduced in Tg-F mice (62.4%), and Tg-F-Abx mice (13.7%) (Fig. 4A). The relative abundance of Bacteroidetes was similar between WT-C and Tg-C mice (5.8% and.6.4%, respectively), but F intake increased it significantly (35.1%) compared to both groups, while antibiotic treatment caused a dramatic reduction of this phylum (1.1%). Proteobacteria was the most predominant *phylum* in antibiotic-treated Tg mice (84.8%) compared to the other groups. No significant differences were seen for Actinobacteria, TM7, and Verrucomicrobia *phyla*. Relative abundances in all groups at the *phylum* and genus (g) level are depicted in Fig. 4A, B, and Table S3. A dramatic increase in *Lactobacillus* (g) (propionate producers; LeBlanc et al. 2017; Ong and Shah 2008; Zhang et al. 2010) was observed in Tg-C compared to WT-C mice (from 30.9 to 50.7% respectively). F intake decreased *Lactobacillus* (g) abundance (from 50.7 to 2.4%, respectively) and increased *Bacteroides* (g), Clostridiales (order; o), *Coprococcus* (g), *Oscillospira* (g), and several butyrate-producing bacteria (i.e., *S24-7*, *Moryella, Dehalobacterium*) compared to Tg-C mice. Antibiotic treatment resulted in a dramatic increase in the relative

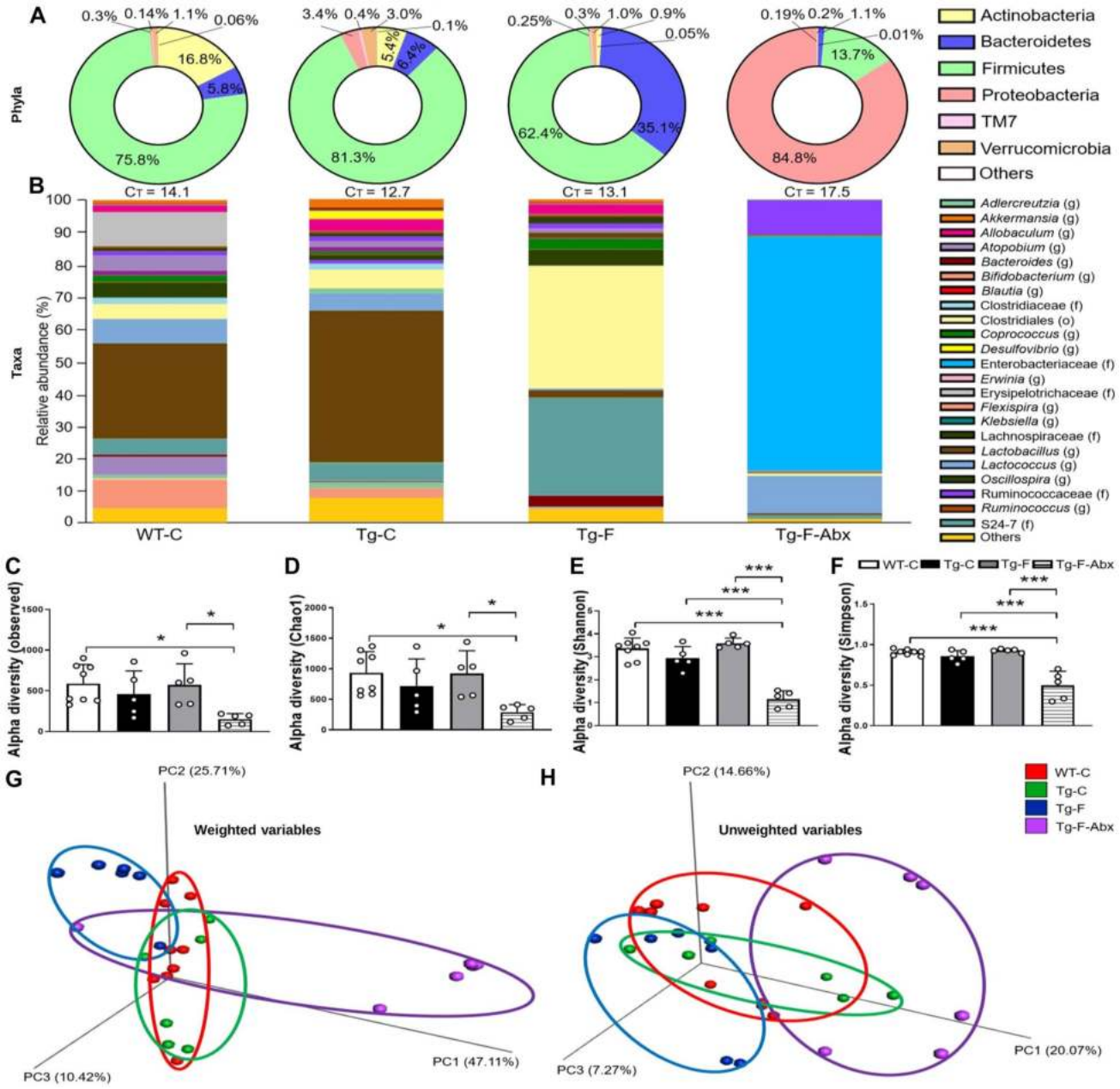

Fig. 4 Relative abundance and microbial diversity of bacterial taxa in fecal samples. **A** Pie charts of Phyla´s relative abundance. Numbers on/beside charts indicate percentages of abundance (out of 100%). The color of each tag on the right side indicates Actinobacteria, Bacteroidetes, Firmicutes, Proteobacteria, TM7, and Verrucomicrobia Phyla. Others are Phyla abundances < 0.1%. **B** Relative abundance of bacterial taxa. The color of each tag on the right side indicates o, f, and g taxa. Others are taxa < 0.5% of relative abundance. CT values indicate the cycle threshold number of the qPCR assay used to calculate bacterial load. Alfa diversity analyses for experimental groups observed as number of taxa [4.24] (**C**), Chao1 richness [4.15] (**D**), Shannon index [37.28] (**E**), and Simpson index [26.71] (**F**). Data between square brackets indicate *F* (DFn, DFd) equivalence values, where DF*n* = 3 and DFd = 19 of one-way ANOVA with Tukey post hoc correction. Beta diversity analyses for experimental groups plotted as principal coordinates analysis (PCoA) of weighted (**G**) and unweighted (**H**) variables. For **A**–B and **G**–**H**, WT-C *n* = 9, Tg-C *n* = 6, Tg-F *n* = 6, and Tg-F-Abx *n* = 6. For C-F, WT-C *n* = 8, Tg-C *n* = 5, Tg-F *n* = 5, and Tg-F-Abx *n* = 5. For **C**–**F**, white color circles within bars indicate experimental subjects. For **A** and **B**, data are shown as mean; complete statistical analyzes and significances are shown in Table S3. For **C**–**F**, data are shown as mean ± SD bars. One-way ANOVA with Tukey post hoc correction; $*p < 0.05$ and $***p < 0.001$. For **G** and **H**, color tags on the right side of the PCoA visual presentation indicate experimental groups and each subject is represented by a color sphere. For **G** and **H**, ADONIS and ANOSIM were performed

abundances of *Enterobacteriaceae* (f) (WT-C = 0.029, Tg-C = 0.025, Tg-F = 0.004 and Tg-F-Abx = 72.990), *Erwinia* (g) (WT-C = 0.008, Tg-C = 0.002, Tg-F = 0.001, and Tg-F-Abx = 10.774), and *Klebsiella* (g) (WT-C = 0.00, Tg-C = 0.00, Tg-F = 0.00, and Tg-F-Abx = 0.16), compared to the rest of the experimental groups (Fig. 4B). Relative abundances at class (c), order, and family levels can be seen in Figure S1 and Table S5.

The alpha diversity is an indicator of a measure of microbiome diversity applicable to a single sample. We estimated the alpha diversity by the observed number of *taxa*, Chao1 richness, and Shannon and Simpson indexes (rarefaction curves are shown in Figure S2 and values for alpha diversity indexes in Table S6). Tg-C mice had a non-significant decreased bacterial diversity compared to the other groups, while Tg-F-Abx mice showed the lowest bacterial diversity compared to WT-C and Tg-F mice (Fig. 4C, D) and the rest of the experimental groups (Fig. 4E, F). An effective bacterial depletion after Abx-treatment was further demonstrated by the cycle threshold (C_T) values (Fig. 4B, S1C, and Table S4). Clustering the bacterial communities using principal coordinates analysis (PCoA) of weighted (Fig. 4G) and unweighted (Fig. 4H) variables revealed that despite clear segregation between experimental groups, only Tg-F-Abx mice had a significantly different gut microbiota than the rest of the groups.

Linear discriminant analysis of the effect size (LEfSe) determines the features most likely to explain differences between groups. We identified several statistical differences ranked by effect size among experimental groups (Fig. 5A). Most prominently, *Lactobacillus* has the highest LDA score in Tg-C mice; Clostridiales and *S24-7* in Tg-F mice; and *Enterobacteriaceae* in Tg-F-Abx mice. Linear discriminant analysis (LDA) values are all shown in Table S7.

Functional metabolic pathways related to mice's fecal microbiota were determined by PICRUSt analysis using the operational taxonomic units (OTU) table (Table S2; OTUs count). Several pathways were generated, but we show only those with significant differences between WT-C, Tg-C, and Tg-F mice (Fig. 5B). The Alzheimer´s disease pathway showed a non-significant increase in Tg-C mice and a non-significant reduction in Tg-F mice, perhaps due to the young age of the animals. However, antibiotic treatment significantly reduced this pathway compared to WT-C and Tg-C mice; this condition can be associated with a reduction in the number of Aβ plaques. Propanoate metabolism was enhanced in Tg-C mice compared to WT-C and Tg-F according to the abundant propionate concentration obtained in fecal samples. Pyruvate metabolism was also increased in Tg-C comparing to WT-C mice, but Tg-F and antibiotic-treated mice showed a dramatic decrease in pyruvate metabolism. LPS biosynthesis increased dramatically in antibiotic-treated mice than in the rest of the groups, in agreement with the obtained LPS plasma levels in this group; this can be associated with an increase in the relative abundance of the gram-negative, pathogen, and proinflammatory bacteria,

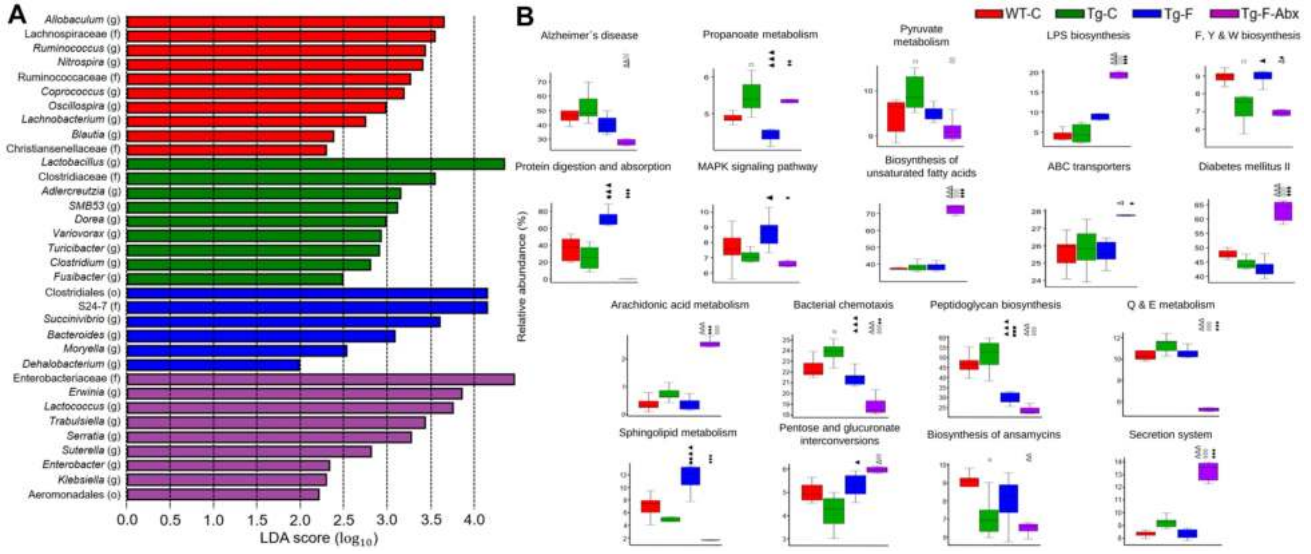

Fig. 5 Enrichment and predictive metabolism of bacterial taxa in fecal samples. **A** Results of LEfSe comparison of differentially abundant bacterial taxa (o, f and g) significantly associated with WT-C, Tg-C, Tg-F, and Tg-F-Abx. Linear discriminant analysis (LDA) score cutoff of 2 was used to discriminate bacterial taxa. Statistical significances are shown in Table S7. **B** Graphic representations of significant predicted metabolic pathways determined by PICRUSt v1.1.1 according to bacterial taxa composition for each experimental group. WT-C $n = 9$, Tg-C $n = 6$, Tg-F $n = 6$, and Tg-F-Abx $n = 6$. Statistical significance between WT-C versus Tg-C (□), WT-C versus Tg-*F* (■), WT-C versus Tg-F-Abx (Δ), Tg-C versus Tg-*F* (▲), Tg-C versus Tg-F-Abx (◊), and Tg-F versus Tg-F-Abx (♦) are indicated by one symbol ($p < 0.05$), two symbols ($p < 0.01$), or three symbols ($p < 0.001$). p and q values are shown in Table S8

such as *Enterobacteriaceae* (Zeng et al. 2017), Aeromonadales (Batra et al. 2016), and *Trabulsiella* (Sapountzis et al. 2015), which are all LPS + *taxa* (Maldonado et al. 2016). Phe, Tyr, and Trp biosynthesis were decreased in the Tg-C mice and Tg-F-Abx groups, but it was increased in Tg-F mice. Protein digestion and absorption pathways increased in Tg-F mice compared to the other groups. ABC transporters and biosynthesis of unsaturated fatty acids were enhanced in Tg-F-Abx mice compared to the other groups. The antibiotic treatment enhances arachidonic acid metabolism, pentose and glucuronate interconversion, and secretion systems compared to WT-C animals. Antibiotic treatment also reduced bacterial chemotaxins, peptidoglycans biosynthesis, D-glutamine and D-glutamate metabolism, sphingolipid metabolism, and biosynthesis of anamysins compared to the other groups. All statistical values of predicted functional metagenome significant pathways are shown in Table S8.

These results indicate that high-fiber intake promotes butyrate producers' survival while reducing the presence of propionate-producing bacteria. Previous work by our group has shown an abundant propionate production and an enhanced propionate concentration in the brain of 9 months-old 3xTGAD mice compared to WT controls (Syeda et al. 2018). In the current study, we were not able to measure SCFAs levels in brain samples; but it is known that SCFAs can be released into the bloodstream and reach the brain (Bélanger et al. 2011; Dalile et al. 2019; Vijay and Morris, 2014), where they are preferentially uptake by astrocytes (Val-Laillet et al. 2018). As we observed that butyrate concentration correlated with few numbers of reactive astrocytes, we evaluated the impact of individual SCFAs on astrocyte metabolism.

Propionate and Butyrate Cause Opposing Effects in Mitochondrial Respiration and Glycolytic Metabolism in Cell Cultures

Cell cultures were used to determine astrocyte glucose uptake using genetically encoded Förster Resonance Energy Transfer nanosensors (AAV9-GFAP- FLII12Pglu700mΔ6) (Takanaga et al. 2008). A dose–response curve was performed to assess the optimal dose of propionate and butyrate for affecting glucose consumption and the glucose depletion rate in astrocytes. Glucose consumption during glucose transport blockage (Cyto B) was higher in astrocytic cells treated with propionate but lower when cells were treated with butyrate (Fig. 6A–C). Glucose depletion rate in the presence of a mitochondrial inhibitor (Azide) was higher when cells were treated with 2 mM propionate, indicating that propionate might be metabolized via glycolysis, causing only mild effects when mitochondria are not fully functional (Fig. 6D). In contrast, when cells were pretreated with butyrate, a lower glucose depletion rate was seen (Fig. 6E). We removed glucose from the perfusion solution to calculate the glucose clearance rate under propionate and butyrate pretreatment. An enhanced glucose clearance was achieved after propionate incubation, but it was reduced in butyrate-treated cells, both compared to controls (Fig. 6F). Our data indicate that propionate and butyrate had differential effects on glucose metabolism in astrocytes, as propionate enhanced the rate of glucose metabolism, but butyrate reduced it. We then aimed to determine the effects of propionate, acetate, and butyrate on mitochondrial respiration and glycolysis by using functional bioenergetics analysis in mouse astrocyte cell cultures.

The oxygen consumption rate (OCR) and the extracellular acidification rate (ECAR) of astrocytes were assessed using an extracellular flux analyzer Seahorse XF96 under a short (2 h; Fig. 7) or long (72 h; Fig. 8) incubation period. We used 1 Mm and 0.5 Mm doses of acetate, propionate, and butyrate. After 2 h incubation period, no significant changes in OCR parameters were seen, except for propionate (1 mM), which increased the spare respiratory capacity, a measure of the ability of the cell to respond to increased energy demands, compared to the control treatment (Fig. 7A, B). Regarding glycolysis, propionate increased the glycolytic reserve under both doses (0.5 mM and 1 mM) (Fig. 7C, D).

A longer incubation period (72 h) caused alterations in OCR parameters, such as basal respiration, ATP-linked respiration, and H^+ leak, which were all increased after acetate and propionate treatments (1 mM). In contrast, butyrate (1 mM) induced the opposite effects as basal respiration, ATP-linked respiration, H + leak, and maximal respiration were all reduced compared to controls (Fig. 8A). Lower propionate concentration (0.5 mM) was enough to cause enhanced basal respiration, ATP-linked respiration, and H + leak compared to control-treated astrocytes. Lower butyrate (0.5 mM) incubation also sufficed to reduce maximal respiration (Fig. 8B). ECAR values showed an enhanced glycolytic capacity and glycolytic reserve after 1 mM and 0.5 mM propionate concentrations compared to controls (Fig. 8C, D). Acetate (1 mM) had a milder effect on increasing the glycolytic reserve, but butyrate (0.5 mM and 1 mM) reduced those parameters compared to propionate (Fig. 8C, D). The differential effects between propionate and butyrate (1 mM; 72 h incubation) in mitochondrial respiration and glycolysis of primary astrocyte cell culture are depicted in Fig. 8E and F. Propionate increased both OCR and ECAR parameters, causing a shift to the right on glycolytic parameters (ECAR) and higher OCR values than butyrate treatment. Based on these data, we conclude that propionate induces a higher metabolic rate in astrocytes (both mitochondrial- dependent and non-mitochondrial-dependent), while butyrate pretreatment causes a quiescent metabolism, resulting in a lower astrocytic metabolic rate (i.e., basal and maximal respiration).

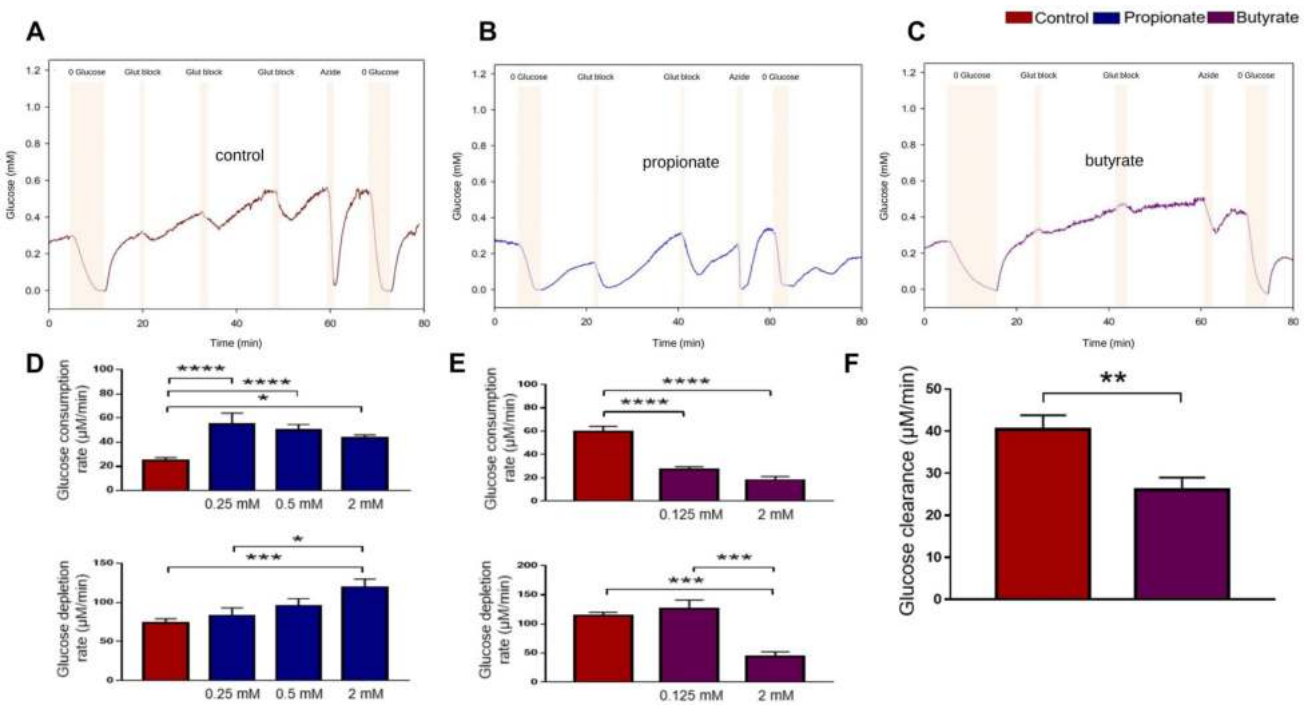

Fig. 6 The effect of propionate and butyrate on astrocytic glycolysis. **A** Changes in intracellular glucose concentration on exposure to zero glucose condition, cyto-B and azide in control (**A**), propionate (**B**), and butyrate (**C**) treated astrocytes. **D** Glucose consumption rate was significantly higher in cells treated with 0.25 mM, 0.5 mM, and 2 mM propionate compared to controls [F (3, 223) = 9.341]. Glucose depletion was higher after 2 mM propionate compared to lower doses (0.25 mM) and controls [F (3, 245) = 5.78]. **E** Glucose consumption rate was significantly lower in cells treated with 0.125 mM and 2 mM butyrate compared to control cells [F (2, 104) = 37.52]. Glucose depletion was significantly lower in cells treated with 2 mM butyrate compared to control cells and compared to 0.125 mM butyrate-treated cells [F (2, 99) = 16.25]. Data between square brackets indicate F (DFn, DFd) values of one-way ANOVA with Tukey post hoc correction. **F** Butyrate (2 mM) pretreatment also reduced glucose clearance compared to control conditions. For **A**–**C**, each line represents data from individual astrocytes, 4 experiments for each condition were performed and 10–15 cells were used for analysis. Data are expressed as the mean ± SD. For **A**–**B** and **D**–**E**, statistical analysis was performed using one-way analysis of variance (ANOVA) with a post hoc Tukey's multiple comparison test. Statistical significances are shown as $*p < 0.05$, $**p < 0.01$, $***p < 0.001$ and $****p < 0.0001$

Discussion

In this study, we demonstrated that by modulating specific gut bacteria throughout the ingestion of fiber (5% fructans from *Agave tequilana*), the unbalanced fecal propionate > butyrate production in Tg mice was restored to WT levels, preventing cognitive impairments. Butyrate concentration was correlated with better cognitive scores in Tg-F mice. In vitro assay proved that propionate enhanced astrocytes' oxidative and glycolytic metabolism, while butyrate induced a quiescent metabolism. Thus, our data indicate that the proportion of gut bacterial-released SCFAs promotes an optimal cognitive function.

Late-onset Alzheimer´s disease is linked to lifestyle risk factors, with diet one of the easiest to be modified. Adopting healthier nutrition has yielded positive outcomes in several clinical studies, as subjects who consume large amounts of vegetables, fruits, fish, and seeds, present a lower conversion to AD or a delayed dementia onset (Gu & Scarmeas 2011). Those diets are composed of multiple components, such as vitamins, antioxidants, bioactive compounds, and fibers. However, some food components may not be accessible all year round, or to the general population. Fiber is a strong modulator of gut bacterial ecology, nourishing and promoting the establishment of commensal bacteria (Chen et al. 2020). Recently, a particular focus has been given to the role of GM on brain health and disease. Consequently, the impact of different fibers on cognition and brain function has been explored. Galactooligosaccharide (GOS) improves exploratory behavior and recognition memory in young pigs by increasing butyrate levels in blood (Fleming et al. 2019). In adult rats, FOS and GOS increase hippocampal BDNF and N-methyl-D-aspartate receptor (NMDAR) NR1 subunit expression.(Savignac et al. 2013). GOS ingestion results in a reduction of brain Aβ 1–42 expression and ameliorates learning and memory deficits in Tg mice (Xin et al. 2018), and an upregulation of synapsin I and PSD-95 while restoring GM in Tg mice (Sun et al. 2020). A probiotic/prebiotic formulation (*E. faecium* + fructans) resulted in improved spatial learning in the WM test, higher BDNF

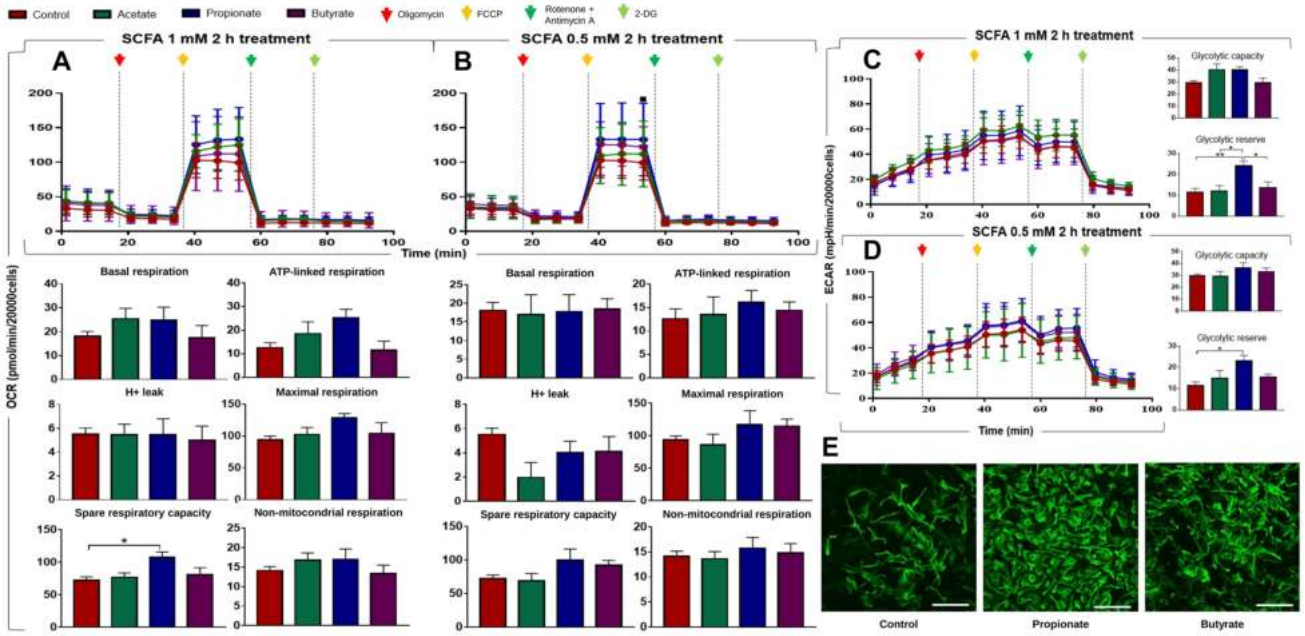

Fig. 7 OCR and ECAR for C57BL/6 primary cortical astrocytes after 2 h incubation with acetate, propionate, or butyrate. OCR profile [F (14, 240) = 69.57 and 97.51], basal respiration [F (3, 16) = 0.902 and 0.028], ATP-linked respiration [F (3, 16) = 2.894 and 0.307], H + leak [F (3, 16) = 0.055 and 2.025], maximal respiration [F (3, 16) = 1.866 and 1.082], spare respiratory capacity [F (3, 16) = 3.702 and 1.841], and non-mitochondrial respiration [F (3, 16) = 0.848 and 0.300] at 1 mM (**A**) and 0.5 mM (**B**) doses of SCFAs after 2 h treatment. ECAR profile [F (14, 240) = 39.94 and 38.07], glycolytic capacity [F (3, 16) = 3.599 and 0.997], and glycolytic reserve [F (3, 16) = 6.188 and 3.885] after 2 h incubation with 1 mM (**C**) and 0.5 mM (**D**) doses of SCFAs. Data between square brackets indicate F (DFn, DFd) values of one-way ANOVA with Tukey post hoc correction for 1- and 0.5-mM doses after 2 h treatment, respectively. **E** Representative images of astrocyte cells immunolabeled with GFAP after pretreatment with propionate and butyrate. Scale bar equals 150 µm. Control, $n = 6$; acetate, $n = 6$; propionate, $n = 6$ and butyrate, $n = 6$. For profiles, circles indicate experimental groups; data are shown as mean $n \pm$ SD bars. Two-way ANOVA followed by Tukey post hoc test; control vs. acetate treatment is shown by □, control vs. propionate treatment by ■, control vs. butyrate treatment by Δ, acetate vs. propionate treatment by ▲, acetate vs. butyrate treatment by ◊, and propionate vs. butyrate treatment by ◆; one symbol $p < 0.05$, two symbols $p < 0.01$, three symbols $p < 0.001$, and four symbols $p < 0.0001$. For metabolic parameters, one-way ANOVA followed by Tukey post hoc analysis; $^{*}p < 0.05$, $^{**}p < 0.01$, $^{***}p < 0.001$, and $^{****}p < 0.0001$

and butyrate levels in middle-aged rats (Romo-Araiza et al. 2018). Despite these prominent data, the mechanism of action of fiber-rich diets in cognitive function has not been fully clarified. Here, we show that a high-fiber diet restores gut dysbiosis and the unbalance propionate: butyrate ratio in an AD-mice model. Butyrate-producing bacteria were enriched in Tg-F mice and consequently enhanced butyrate concentration. This condition resulted in better working and spatial memory and reduced anxiety in male Tg mice.

Butyrate targets many pathways with multiple mechanisms of action in brain cells. Butyrate inhibits histone-deacetylation modulating gene expression in neurons and glia cells (Huuskonen et al. 2004; Shukla & Tekwani 2020). Butyrate supplementation increases neurogenesis in the hippocampus of adult pigs (Val-Laillet et al. 2018), reduces apoptosis in cerebral ischemia/reperfusion mice model (Sun et al. 2015), and promotes synaptic plasticity in 5xFAD mice (Jiang et al. 2021). Butyrate administration attenuates microglia activation in APP/PS1 mice (Sun et al. 2020). Microglia have been positioned as a key player in the microbiota-gut-brain axis, as antibiotic treatment impacts not only Aβ deposition but also microglia activation (Minter et al. 2016, 2017) and maturation (Erny et al. 2015; Wang et al. 2018). The relationship between GM and astrocyte function is just being described, with complex interactions from metabolic bioproducts to modulation of the neuroimmune system. Gut bacteria metabolites suppress neuroinflammation by activation of aryl hydrocarbon receptor signaling in astrocytes (Rothhammer et al. 2016; Sanmarco et al. 2021) (Rothhammer et al. 2016; Sanmarco et al. 2021), and GM regulates the expression of genes involved in the astrocyte-neuron lactate shuttle in the hippocampus (Margineanu et al. 2020). In 3XADTg mice, gut dysbiosis was accompanied by an exacerbated production of propionate and astrocyte activation (Syeda et al. 2018). Astrocytes are key modulators of brain metabolism and function, responsible for glucose entrance into the brain (Colombo and Farina 2016; Deitmer et al. 2019). Furthermore, astrocytes can actively clear Aβ and degrade it (Xiao et al. 2014). In advanced stages of AD, the neuroprotective role of active

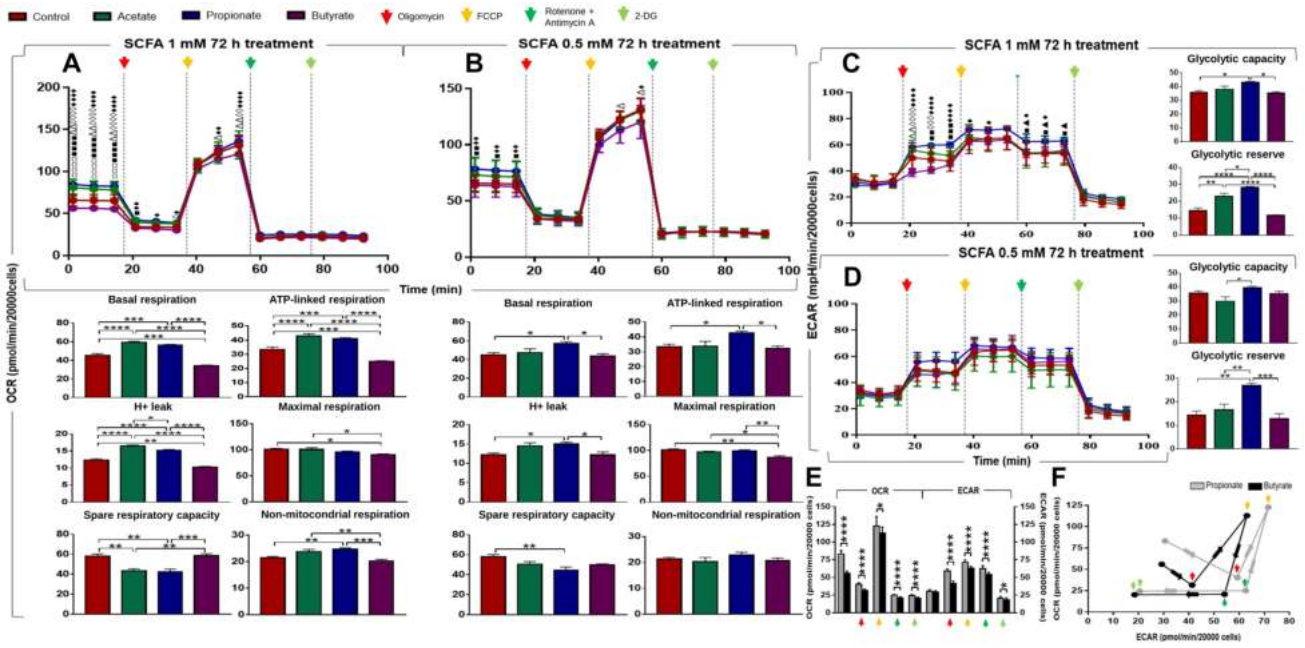

Fig. 8 OCR and ECAR for C57BL/6 primary cortical astrocytes after 72 h incubation with acetate, propionate, or butyrate. OCR profile [F (14, 240) = 1361 and 763.4], basal respiration [F (3, 16) = 64.97 and 4.94], ATP-linked respiration [F (3, 16) = 53.66 and 4.778], H + leak [F (3, 16) = 76.75 and 4.794], maximal respiration [F (3, 16) = 4.497 and 8.921], spare respiratory capacity [F (3, 16) = 14.54 and 5.611], and non-mitochondrial respiration [F (3, 16) = 10.36 and 1.068] at 1 mM (**A**) and 0.5 mM (**B**) doses of SCFAs after 72 h treatment. ECAR profile [F (14, 300) = 244.6, and 114.9], glycolytic capacity [F (3, 16) = 5.300, and 3.904], and glycolytic reserve [F (3, 16) = 35.03 and 11.51] after 72 h incubation with 1 mM (**C**) and 0.5 mM (D) doses of SCFAs. Data between square brackets indicate F (DFn, DFd) values of one-way ANOVA with Tukey post hoc correction for 1- and 0.5-mM doses after 72 h treatment, respectively. (**E**) Differences between OCR and ECAR values before oxidative and glycolytic cellular effectors and after oligomycin, FCCP, rotenone and antimycin A, and 2-DG. (**F**) Bioenergetic profiling of C57BL/6 primary cortical astrocytes. Circles indicate OCR and ECAR interceptions before oxidative and glycolytic cellular effectors and after oligomycin, FCCP, rotenone and antimycin A, and 2-DG exposition. Control, $n = 6$; acetate, $n = 6$; propionate, $n = 6$ and butyrate, $n = 6$. For profiles, circles indicate experimental groups; data are shown as mean ± SD bars. Two-way ANOVA followed by Tukey post hoc test; control vs. acetate treatment is shown by □, control vs. propionate treatment by ■, control vs. butyrate treatment by Δ, acetate vs. propionate treatment by ▲, acetate vs. butyrate treatment by ◊, and propionate vs. butyrate treatment by ◆; one symbol $p < 0.05$, two symbols $p < 0.01$, three symbols $p < 0.001$, and four symbols $p < 0.0001$. For metabolic parameters, one-way ANOVA followed by Tukey post hoc analysis; $^{*}p < 0.05$, $^{**}p < 0.01$, $^{***}p < 0.001$, and $^{****}p < 0.0001$. For **E**, data are shown as mean ± SD bars; unpaired parametric multiple t test indicate $^{*}p < 0.05$, $^{**}p < 0.01$, $^{***}p < 0.001$, and $^{****}p < 0.0001$. For F, data are shown as mean

astrocytes is disrupted, as reactive astrocytes and the released pro-inflammatory cytokines provoke neuronal damage and synapse degeneration (Lue et al. 1996; Perez-Nievas et al. 2013). In this study, we observed an altered proportion of the three main fecal SCFAs (acetate: propionate: butyrate) in Tg-C mice compared to WT-C mice (WT-C: 81.5%: 9.5%: 9.0%; Tg-C: 55.8%: 37.6%: 6.6%, respectively), but it was restored to control values after high-fiber intake (Tg-F: 75.0%: 14.0%: 11.0%). The effects of propionate are extremely broad, influencing several biochemical processes (metabolism, gene expression, receptors, mitochondria function) that are not only dose- and time-dependent but also cellular-specific. Propionate causes an increased number of reactive astrocytes (De Almeida et al. 2006) (De Almeida et al. 2006) and neuroinflammation (MacFabe et al. 2007; MacFabe 2015) (MacFabe 2015; MacFabe et al. 2007). In cell culture, propionate induced the expression of IL-22 in astrocytes (Spichak et al. 2021). (Spichak et al. 2021). IL-22 expression promotes astrocyte survival by decreased apoptosis (Perriard et al. 2015). In lymphoblastoid cells, propionate (0.1 mM for 24 h) elevates ATP-linked respiration, maximal respiratory capacity, and reserve capacity. However, longer exposure periods enhance proton leakage linked to ROS generation and mitochondrial dysfunction (Frye et al. 2016). An excess of propionate increases susceptibility to abiotic stress and bacterial pathogenesis (Revtovich et al. 2019). Moreover, propionate´s systemic administration results in alterations in social behavior and working memory impairments (MacFabe et al. 2007). Fecal samples of children with autism spectrum disorder show a higher abundance of propionate producers (Wang et al. 2018), and Propionic Acidemia patients show higher fecal propionate concentrations related to cognitive impairments (Gallego-Villar et al. 2013; Sethi et al. 1989; Morland et al.

2018; Scott Schwoerer et al. 2018). Furthermore, in AD patients, increased propionate and acetate levels are found in saliva compared to healthy controls (Figueira et al. 2016; Yilmaz et al. 2017), and fecal microbiota transplant from AD patients to healthy mice results in higher levels of propionate than fecal transplantation from healthy volunteers (Fujii et al. 2019). Therefore, our results support previous data and indicate that propionate enhances astrocytic metabolism and is overproduction might be involved in AD etiology (Killingsworth et al. 2021).

Previous reports showed that antibiotic treatment depletes GM, but it also causes a reduction of amyloid plaques in Tg mice (Dodiya et al. 2019; Minter et al. 2016). However, soluble Aβ concentration increases in antibiotic-treated Tg mice (Jendresen et al. 2019). Our antibiotic protocol effectively diminished GM diversity and abundance, causing a predominant enrichment of *Enterobacteriaceae* and altered intestinal morphology that may lead to a leaky gut. Tg-F-Abx mice had a diminished number of Aβ plaques in the hippocampus a two-fold increased LPS plasma levels, but presented impaired cognitive performance. Similarly, Fröhlich et al. (2016) reported that similar antibiotic treatment causes recognition memory dysfunction in conventional mice. We also observed that antibiotic treatment resulted in fewer reactive astrocytes in the hippocampus of Tg-F-Abx than in Tg-C mice. Reduced diversity of butyrate-producing bacteria resulted in lower butyrate concentration in Tg-F-Abx mice. Notwithstanding, the antibiotic treatment also depleted propionate-producing bacteria and reduced propionate concentration. As mentioned before, propionate is a potent neurotoxic substance that cause astrocyte activation. Accordingly, low levels of this neurotoxic substance may be associated with few reactive astrocytes in Tg-F-Abx. However, similarly to the reduced number of amyloid plaques after antibiotic-treatment, the reduced number of reactive astrocytes observed in Tg-F-Abx mice was not accompanied by an improved cognitive function. On the contrary, butyrate levels were highly enriched in Tg-F mice and correlated well with memory function; a condition lost after antibiotic treatment. Besides SCFAs production, GM modulation by a high-fiber diet was related to different bacteria products that interact with host physiology as described by the predicted metabolic by functional metagenome (PICRUS) (Fig. 5). Pyruvate, propanoate, and LPS were enhanced metabolic pathways in Tg-C mice, but Phe, Tyr, and Trp biosynthesis were decreased and further restored in Tg-F mice. AD patients show a decrease in Trp metabolites (Wu et al. 2021; Whiley et al. 2021), a condition that is aggravated by disease severity (Shao et al. 2020). It has been postulated that Trp metabolites modulate amyloid aggregation and glia activation (Ano et al. 2019; Weaver et al. 2020). Moreover, Trp pathways metabolized by GM are altered in AD patients (Wu et al. 2021). Our data fit well with these reports and may also relate to the reduced anxiety scores observed in Tg-F mice, as a reduction in anxiety symptoms is achieved by the use of a high Trp in the diet (Lindseth et al. 2015). Further studies are needed to identify these bacterial metabolites in mice fed with fructans to dissect better other metabolic and cellular targets that may be involved in the neuroprotective effects of the diet.

We used FRET-glucose nanosensors selectively expressed in astrocytes to understand better the impact of each SCFAs on the astrocyte´s metabolism. Propionate enhanced glucose consumption when glucose entrance was blocked. Contrary, butyrate decreased glucose consumption and depletion rates under the same conditions; this indicates a higher glucose utilization by astrocytes under propionate incubation. Then, we explored the impact of each SCFAs on glycolytic and oxidative metabolic profiles using primary astrocyte cultures. Propionate and acetate incubation induced a higher OCR values associated with increased ECAR compared to the control treatment. Propionate produced a more robust effect indicating a pronounced astrocytic energy demand under this condition. In contrast, butyrate decreased basal respiration, maximal respiration, ATP-linked respiration, and H + leak, associated with lower OCR and ECAR values. Thus, butyrate incubation shifted the metabolic rate to a more quiescent state. Astrocytes prefer a glycolytic metabolism, which is increased after activation (Bélanger et al. 2011). Propionate is metabolized oxidatively by astrocytes (Nguyen et al. 2007), impairing the TCA and interfering with the generation of succinyl Co-A from succinate, leading to mitochondrial dysfunction (Mehan et al. 2020). Acetate is preferentially uptaken by astrocytes (Wyss et al. 2011; Waniewski and Martin 1998), and [14C] acetate reaches glutamate, which is later converted to glutamine in astrocytes (Waniewski and Martin 1998). Acetate causes mitochondrial stress in astrocytes (Kretschmer et al. 2018), but it does not necessarily produce detrimental effects in vivo (Reick et al. 2016; Gibbs et al. 2008). Beta-hydroxybutyrate (BHB), a ketone body, inhibits the glycolytic pathway in primary astrocytes (Valdebenito et al. 2016), similar to our current results with the SCFA butyrate. Therefore, our data indicate that propionate and acetate increase astrocyte metabolism, while butyrate promotes a more resting state.

In conclusion, here we demonstrate that ingestion of fructans (5%) for two months effectively reshaped the gut microbiota´s ecology, promoting the abundance of butyrate producers and depleting propionate linked-bacteria, with a consequent cognitive improvement in male Tg mice. Fructans intake can be a promising therapy to prevent a dysbiotic microbiome in people at risk to develop AD. Furthermore, fructans can be easily accessible and well-tolerated by the general population (Ramnani et al. 2015). Our data add further information to understand better the mechanism of action of a healthy diet in preventing dementia and AD.

We highly recommend determining SCFAs levels before and during a dietary intervention aimed to reshape the GM to ensure an optimal cognitive function.

Supplementary Information The online version contains supplementary material available at https://doi.org/10.1007/s10571-022-01268-7.

Acknowledgements Thanks to Alberto Piña-Escobedo for assistance with semiconductor DNA sequencing, to Rodrigo García-Gutierrez with reagents, Viridana Rosas-Ocegueda administrative assistance, and Gustavo Bustillo Armendáriz (Bustar Foods) for fructans donation.

Author contributions Conceptualization, C.P.C. and J.G.M.; Methodology, D.C.Z., T.S., V.S.V, M.I.F., P.T.A., A.S.O., I.R.; Investigation, M.T.R., M.S.S., L.G.N., N.T., and A.R.T; Writing – Original Draft, C.P.C and D.C.Z; Writing – Review & Editing, C.P.C and J.G.M.; Funding Acquisition, C.P.C. and J.G.M.; Resources, C.P.C., J.G.M., N.T., A.T.; Supervision, C.P.C and J.G.M.

Funding D.C.Z. and T.S. received a Ph.D. scholarship CONACyT-Mexico. CONACYT Grant No. A1S-42600 and CINVESTAV Grant No.128 for C.P.C, CONACYT Grant No. 163235 INFR-2011-01 for J.G.M. CECs is funded by the Chilean Government through the Centers of Excellence Basal Financing Program of ANID.

Data Availability All sequencing data generated in this study are deposited at NCBI sequence read archive repository as bioproject PRJNA718599 (https://www.ncbi.nlm.nih.gov/Traces/study/?acc=PRJNA718599), and are publicly available as of the date of publications. Any additional information required to reanalyze the data reported in this paper is available from the lead contact upon request.

Declarations

Competing interests The authors declare no conflict of interests.

References

Abdelli LS, Samsam A, Naser SA (2019) Propionic acid induces gliosis and neuro-inflammation through modulation of PTEN/AKT pathway in autism spectrum disorder. Sci Rep 9(1):1–12. https://doi.org/10.1038/s41598-019-45348-z

Akiyama H, Barger S, Barnum S, Bradt B, Bauer J, Cole GM, Cooper NR, Eikelenboom P, Emmerling M, Fiebich BL, Finch CE, Frautschy S, Griffin WS, Hampel H, Hull M, Landreth G, Lue L, Mrak R, Mackenzie IR, Mc T (2000) Systemic inflammation and Alzheimer's disease. Neurobiol Aging 21(3):383–421. https://doi.org/10.1042/BST0390898

Anderson JW (1990) Plant fiber in foods, 2nd edn. HCF Nutrition Research Foundation Inc, Lexington

Annison G, Illman RJ, Topping DL (2003) Acetylated, propionylated or butyrylated starches raise large bowel short-chain fatty acids preferentially when fed to rats. J Nutr 133(11):3523–3528. https://doi.org/10.1093/jn/133.11.3523

Ano Y, Yoshino Y, Uchida K, Nakayama H (2019) Preventive effects of tryptophan–methionine dipeptide on neural inflammation and alzheimer's pathology. Int J of Mol Sci. https://doi.org/10.3390/ijms20133206

Batra P, Mathur P, Misra MC (2016) Aeromonas spp.: an emerging nosocomial pathogen. J Labor Phys 8(01):001–004. https://doi.org/10.4103/0974-2727.176234

Bélanger M, Allaman I, Magistretti PJ (2011) Brain energy metabolism: focus on astrocyte-neuron metabolic cooperation. Cell Metab 14(6):724–738. https://doi.org/10.1016/j.cmet.2011.08.016

Binley KE, Ng WS, Tribble JR, Song B, Morgan JE (2014) Sholl analysis: a quantitative comparison of semi-automated methods. J Neurosci Methods 225:65–70. https://doi.org/10.1016/j.jneumeth.2014.01.017.Access

Caporaso JG, Kuczynski J, Stombaugh J, Bittinger K, Bushman FD, Costello EK, Fierer N, Peña AG, Goodrich JK, Gordon JI, Huttley GA, Kelley ST, Knights D, Koenig JE, Ley RE, Lozupone CA, McDonald D, Muegge BD, Pirrung M, Reeder J, Sevinsky JR, Turnbaugh PJ (2010) QIIME allows analysis of high-throughput community sequencing data. Nat Methods 7(5):335–336. https://doi.org/10.1038/nmeth.f.303.QIIME

Cattaneo A, Cattane N, Galluzzi S, Provasi S, Lopizzo N, Festari C, Ferrari C, Guerra UP, Paghera B, Muscio C, Bianchetti A, Volta GD, Turla M, Cotelli MS, Gennuso M, Prelle A, Zanetti O, Lussignoli G, Mirabile D et al (2017) Association of brain amyloidosis with pro-inflammatory gut bacterial taxa and peripheral inflammation markers in cognitively impaired elderly. Neurobiol Aging 49:60–68. https://doi.org/10.1016/j.neurobiolaging.2016.08.019

Chen M, Fan B, Liu S, Imam KMSU, Xie Y, Wen B, Xin F (2020) The in vitro effect of fibers with different degrees of polymerization on human gut bacteria. Front Microbiol 11(May):1–12. https://doi.org/10.3389/fmicb.2020.00819

Colombo E, Farina C (2016) Astrocytes: key regulators of neuroinflammation. Trends Immunol 37(9):608–620. https://doi.org/10.1016/j.it.2016.06.006

Corona-Cervantes K, García-González I, Villalobos-Flores LE, Hernández-Quiroz F, Piña-Escobedo A, Hoyo-Vadillo C, Rangel-Calvillo MN, García-Mena J (2020) Human milk microbiota associated with early colonization of the neonatal gut in Mexican newborns. PeerJ. https://doi.org/10.7717/peerj.9205

Dalile B, Van-Oudenhove L, Vervliet B, Verbeke K (2019) The role of short-chain fatty acids in microbiota–gut–brain communication. Nat Rev Gastroenterol Hepatol 16(8):461–478. https://doi.org/10.1038/s41575-019-0157-3

Erny D, Hrabě AL, de Angelis D, Jaitin PW, Staszewski O, David E, Keren-Shaul H, Mahlakoiv T, Jakobshagen K, Buch T, Schwierzeck V, Utermöhlen O, Chun E, Garrett WS, McCoy KD (2015) Host microbiota constantly control maturation and function of microglia in the CNS. Physiol Behav 176(5):139–148. https://doi.org/10.1016/j.physbeh.2017.03.040

Das KC (2013) Hyperoxia decreases glycolytic capacity, glycolytic reserve and oxidative phosphorylation in MLE-12 cells and inhibits complex I and II function, but not complex IV in isolated mouse lung mitochondria. PLoS ONE. https://doi.org/10.1371/journal.pone.0073358

De Almeida LMV, Funchal C, Gottfried C, Wajner M, Pessoa-Pureur R (2006) Propionic acid induces cytoskeletal alterations in cultured astrocytes from rat cerebral cortex. Metab Brain Dis 21(1):51–62. https://doi.org/10.1007/s11011-006-9002-9

De Baere S, Eeckhaut V, Steppe M, De Maesschalck C, De Backer P, Van Immerseel F, Croubels S (2013) Development of a HPLC-UV method for the quantitative determination of four short-chain fatty acids and lactic acid produced by intestinal bacteria during in vitro fermentation. J Pharmac Biomed Anal 80:107–115. https://doi.org/10.1016/j.jpba.2013.02.032

Deacon RMJ, Rawlins JNP (2006) T-maze alternation in the rodent. Nat Protoc 1(1):7–12. https://doi.org/10.1038/nprot.2006.2

Deitmer JW, Theparambil SM, Ruminot I, Noor SI, Becker HM (2019) Energy dynamics in the brain: contributions of astrocytes to metabolism and pH homeostasis. Front Neurosci 13(December):1–7. https://doi.org/10.3389/fnins.2019.01301

Divakaruni AS, Paradyse A, Ferrick DA, Murphy AN, Jastroch M (2014) Analysis and interpretation of microplate-based oxygen consumption and pH data. In: Methods in enzymology, 1st edn, vol 547, issue C. Elsevier Inc. https://doi.org/10.1016/B978-0-12-801415-8.00016-3

Dodiya HB, Kuntz T, Shaik SM, Baufeld C, Leibowitz J, Zhang X, Gottel N, Zhang X, Butovsky O, Gilbert JA, Sisodia SS (2019) Sex-specific effects of microbiome perturbations on cerebral Ab amyloidosis and microglia phenotypes. J Exp Med 216(7):1542–1560. https://doi.org/10.1084/jem.20182386

Donohoe DR, Garge N, Zhang X, Sun W, O'Connell TM, Bunger MK, Bultman SJ (2011) The microbiome and butyrate regulate energy metabolism and autophagy in the mammalian colon. Cell Metab 13(5):517–526. https://doi.org/10.1016/j.cmet.2011.02.018

Engelhart MJ, Geerlings MI, Meijer J, Kiliaan A, Ruitenberg A, van Swieten JC, Stijnen T, Hofman A, Witteman JC, Breteler MM (2004) Inflammatory proteins in plasma and the risk of dementia: the Rotterdam study. Arch Neurol 61(5):668–672

Escudero-Lourdes C, Uresti-Rivera EE, Oliva-González C, Torres-Ramos MA, Aguirre-Bañuelos P, Gandolfi AJ (2016) Cortical astrocytes acutely exposed to the monomethylarsonous acid (MMAIII) show increased pro-inflammatory cytokines gene expression that is consistent with APP and BACE-1: over-expression. Neurochem Res 41(10):2559–2572. https://doi.org/10.1007/s11064-016-1968-z

Fernández-Martínez E, Jiménez-Santana M, Centeno-Álvarez M, Torres-Valencia JM, Shibayama M, Cariño-Cortés R (2018) Hepatoprotective effects of nonpolar extracts from inflorescences of thistles *Cirsium vulgare* and *Cirsium ehrenbergii* on acute liver damage in rat. Pharmacogn Mag 31(Suppl 4):S860–S867. https://doi.org/10.4103/pm.pm

Figueira J, Jonsson P, Nordin Adolfsson A, Adolfsson R, Nyberg L, Öhman A (2016) NMR analysis of the human saliva metabolome distinguishes dementia patients from matched controls. Mol BioSyst 12(8):2562–2571. https://doi.org/10.1039/C6MB00233A

Fleming SA, Monaikul S, Patsavas AJ, Waworuntu RV, Berg BM, Dilger RN (2019) Dietary polydextrose and galactooligosaccharide increase exploratory behavior, improve recognition memory, and alter neurochemistry in the young pig. Nutr Neurosci 22(7):499–512. https://doi.org/10.1080/1028415X.2017.1415280

Fröhlich EE, Farzi A, Mayerhofer R, Reichmann F, Jačan A, Wagner B, Zinser E, Bordag N, Magnes C, Fröhlich E, Kashofer K, Gorkiewicz G, Holzer P (2016) Cognitive impairment by antibiotic-induced gut dysbiosis: analysis of gut microbiota-brain communication. Brain Behav Immun 56:140–155. https://doi.org/10.1016/j.bbi.2016.02.020

Frye RE, Rose S, Chacko J, Wynne R, Bennuri SC, Slattery JC, Tippett M, Delhey L, Melnyk S, Kahler SG, MacFabe DF (2016) Modulation of mitochondrial function by the microbiome metabolite propionic acid in autism and control cell lines. Transl Psychiatry 6(10):e927–e1010. https://doi.org/10.1038/tp.2016.189

Fujii Y, Nguyen TTT, Fujimura Y, Kameya N, Nakamura S, Arakawa K, Morita H (2019) Fecal metabolite of a gnotobiotic mouse transplanted with gut microbiota from a patient with Alzheimer's disease. Biosci Biotechnol Biochem 83(11):2144–2152. https://doi.org/10.1080/09168451.2019.1644149

Gallego-Villar L, Pérez-Cerdá C, Pérez B, Abia D, Ugarte M, Richard E, Desviat LR (2013) Functional characterization of novel genotypes and cellular oxidative stress studies in propionic acidemia. J Inherit Metab Dis 36(5):731–740. https://doi.org/10.1007/s10545-012-9545-3

Gibbs M, Lloyd H, Thomas Santa LH (2008) Glycogen is a preferred glutamate precursor during learning in 1-day-old chick: biochemical and behavioral evidence. J Neurosci Res 85(15):3326–3333. https://doi.org/10.1002/jnr

Gibson GR, Hutkins R, Sanders ME, Prescott SL, Reimer RA, Salminen SJ, Scott K, Stanton C, Swanson KS, Cani PD, Verbeke K, Reid G (2017) Expert consensus document: The International Scientific Association for Probiotics and Prebiotics (ISAPP) consensus statement on the definition and scope of prebiotics. Nat Rev Gastroenterol Hepatol 14(8):491–502. https://doi.org/10.1038/nrgastro.2017.75

González-Reyes RE, Nava-Mesa MO, Vargas-Sánchez K, Ariza-Salamanca D, Mora-Muñoz L (2017) Involvement of astrocytes in Alzheimer's disease from a neuroinflammatory and oxidative stress perspective. Front Mol Neurosci 10(December):1–20. https://doi.org/10.3389/fnmol.2017.00427

Gu Y, Scarmeas N (2011) Dietary patterns in Alzheimers disease and cognitive aging. Curr Alzheimer Res 8(5):510–519. https://doi.org/10.2174/156720511796391836

Guan ZW, Yu EZ, Feng Q (2021) Soluble dietary fiber, one of the most important nutrients for the gut microbiota. Molecules 26(22):1–15. https://doi.org/10.3390/molecules26226802

Guo JP, Arai T, Miklossy J, McGeer PL (2006) Abeta and tau form soluble complexes that may promote self aggregation of both into the insoluble forms observed in Alzheimer's disease. Proc Natl Acad Sci USA 103(6):1953–1958

Huazano-Garcia A, López GM (2013) Metabolism of short chain fatty acids in the colon and faeces of mice after a supplementation of diets with agave fructans. Lipid Metabol. https://doi.org/10.5772/51248

Huuskonen J, Suuronen T, Nuutinen T, Kyrylenko S, Salminen A (2004) Regulation of microglial inflammatory response by sodium butyrate and short-chain fatty acids. Br J Pharmacol 141(5):874–880. https://doi.org/10.1038/sj.bjp.0705682

Jendresen C, Digre A, Cui H, Zhang X, Vlodavsky I, Li JP, Nilsson LNG (2019) Systemic LPS-induced Aβ-solubilization and clearance in AβPP-transgenic mice is diminished by heparanase overexpression. Sci Rep 9(1):1–12. https://doi.org/10.1038/s41598-019-40999-4

Jiang Y, Li K, Li X, Xu L, Yang Z (2021) Sodium butyrate ameliorates the impairment of synaptic plasticity by inhibiting the neuroinflammation in 5XFAD mice. Chem Biol Interact 341(March):109452. https://doi.org/10.1016/j.cbi.2021.109452

Kanski R, Sneeboer MAM, van Bodegraven EJ, Sluijs JA, Kropff W, Vermunt MW, Creyghton MP, de Filippis L, Vescovi A, Aronica E, van Tijn P, van Strien ME, Hol EM (2014) Histone acetylation in astrocytes suppresses GFAP and stimulates a reorganization of the intermediate filament network. J Cell Sci 127(20):4368–4380. https://doi.org/10.1242/jcs.145912

Kashon ML, Ross GW, O'Callaghan JP, Miller DB, Petrovitch H, Burchfiel CM, Sharp DS, Markesbery WR, Davis DG, Hardman J, Nelson J, White LR (2004) Associations of cortical astrogliosis with cognitive performance and dementia status. J Alzheimer's Dis 6(6):595–604. https://doi.org/10.3233/jad-2004-6604

Khandelwal PJ, Herman AM, Moussa CEH (2011) Inflammation in the early stages of neurodegenerative pathology. J Neuroimmunol 238(1–2):1–11. https://doi.org/10.1016/j.jneuroim.2011.07.002

Killingsworth J, Sawmiller D, Shytle RD (2021) Propionate and Alzheimer's Disease. Front Aging Neurosci 12(January):1–10. https://doi.org/10.3389/fnagi.2020.580001

Kretschmer M, Lambie S, Croll D, Kronstad JW (2018) Acetate provokes mitochondrial stress and cell death in Ustilago maydis. Mol Microbiol 107(4):488–507. https://doi.org/10.1111/mmi.13894

Langille MGI, Zaneveld J, Caporaso JG, McDonald D, Knights D, Reyes JA, Clemente JC, Burkepile DE, Vega Thurber RL, Knight R, Beiko RG, Huttenhower C (2013) Predictive functional profiling of microbial communities using 16S rRNA marker gene sequences. Nat Biotechnol 31(9):814–821. https://doi.org/10.1038/nbt.2676

Le Douce J, Maugard M, Veran J, Matos M, Jégo P, Vigneron PA, Faivre E, Toussay X, Vandenberghe M, Balbastre Y, Piquet J, Guiot E, Tran NT, Taverna M, Marinesco S, Koyanagi A, Furuya S, Gaudin-Guérif M, Goutal S et al (2020) Impairment of glycolysis-derived L-serine production in astrocytes contributes to cognitive deficits in Alzheimer's disease. Cell Metab 31(3):503-517.e8. https://doi.org/10.1016/j.cmet.2020.02.004

LeBlanc JG, Chain F, Martín R, Bermúdez-Humarán LG, Courau S, Langella P (2017) Beneficial effects on host energy metabolism of short-chain fatty acids and vitamins produced by commensal and probiotic bacteria. Microb Cell Fact 16(1):1–10. https://doi.org/10.1186/s12934-017-0691-z

Levrat MA, Remesy C, Demigne C (1991) High propionic acid fermentations and mineral accumulation in the cecum of rats adapted to different levels of inulin. J Nutr 121(11):1730–1737. https://doi.org/10.1093/jn/121.11.1730

Li C, Zhao R, Gao K, Wei Z, Yaoyao YM, Ting LL, Chui D, Cheung HYA (2011) Astrocytes: implications for neuroinflammatory pathogenesis of Alzheimers disease. Curr Alzheimer Res 8(1):67–80. https://doi.org/10.2174/156720511794604543

Lue L-F, Libuse Brachova W, Harold Civin JR (1996) Inflammation, Aβ deposition, and neurofibrillary tangle formation as correlates of Alzheimer´s disease neurodegeneration. J Neuropathol Exp Neurol 55(10):1083–1088

Lim YY, Maruff P, Pietrzak RH, Ames D, Ellis KA, Harrington K, Lautenschlager NT, Szoeke C, Martins RN, Masters CL, Villemagne VL, Rowe CC (2014) Effect of amyloid on memory and non-memory decline from preclinical to clinical Alzheimer's disease. Brain 137(1):221–231. https://doi.org/10.1093/brain/awt286

Lindseth G, Helland B, Caspers J (2015) The effects of dietary tryptophan on affective disorders. Arch Psychiatr Nurs 29(2):102–107. https://doi.org/10.1016/j.apnu.2014.11.008

Liu P, Wu L, Peng G, Han Y, Tang R, Ge J, Zhang L, Jia L, Yue S, Zhou K, Li L, Luo B, Wang B (2019) Altered microbiomes distinguish Alzheimer's disease from amnestic mild cognitive impairment and health in a Chinese cohort. Brain Behav Immun 80:633–643. https://doi.org/10.1016/j.bbi.2019.05.008

Lu J, Guo P, Liu X, Zhang Y, Guo X, Gao X, Chen Y (2019) Herbal formula Fo Shou San attenuates Alzheimer's disease-related pathologies via the gut-liver-brain axis in APP/PS1 mouse model of Alzheimer's disease. Evid-Based Complement Alternat Med. https://doi.org/10.1155/2019/8302950

MacFabe DF (2015) Enteric short-chain fatty acids: microbial messengers of metabolism, mitochondria, and mind: implications in autism spectrum disorders. Microb Ecol Health Dis 26:1–14. https://doi.org/10.3402/mehd.v26.28177

MacFabe DF, Cain DP, Rodriguez-Capote K, Franklin AE, Hoffman JE, Boon F, Taylor AR, Kavaliers M, Ossenkopp KP (2007) Neurobiological effects of intraventricular propionic acid in rats: possible role of short chain fatty acids on the pathogenesis and characteristics of autism spectrum disorders. Behav Brain Res 176(1):149–169. https://doi.org/10.1016/j.bbr.2006.07.025

Macfarlane S, Macfarlane GT (2003) Regulation of short-chain fatty acid production. Proc Nutr Soc 62(1):67–72. https://doi.org/10.1079/pns2002207

Maldonado RF, Isabel S, Valvano MA (2016) Lipopolysaccharide modification in Gram-negative. FEMS Microbiol Rev 40:480–493. https://doi.org/10.1093/femsre/fuw007

Margineanu MB, Sherwin E, Golubeva A, Peterson V, Hoban A, Fiumelli H, Rea K, Cryan JF, Magistretti PJ (2020) Gut microbiota modulates expression of genes involved in the astrocyte-neuron lactate shuttle in the hippocampus. Eur Neuropsychopharmacol 41:152–159. https://doi.org/10.1016/j.euroneuro.2020.11.006

Medina-Buelvas DM, Estrada-Muñiz E, Rodríguez-Sosa M, Shibayama M, Vega L (2019) Increased heart fibrosis and acute infection in a murine Chagas disease model associated with organophosphorus pesticide metabolite exposure. Sci Rep 9(1):1–12. https://doi.org/10.1038/s41598-019-54218-7

Mehan S, Rahi S, Tiwari A, Kapoor T, Rajdev K, Sharma R, Khera H, Kosey S, Kukkar U, Dudi R (2020) Adenylate cyclase activator forskolin alleviates intracerebroventricular propionic acid-induced mitochondrial dysfunction of autistic rats. Neural Regen Res 15(6):1140–1149. https://doi.org/10.4103/1673-5374.270316

Minter MR, Hinterleitner R, Meisel M, Zhang C, Leone V, Zhang X, Oyler-Castrillo P, Zhang X, Musch MW, Shen X, Jabri B, Chang EB, Tanzi RE, Sisodia SS (2017) Antibiotic-induced perturbations in microbial diversity during post-natal development alters amyloid pathology in an aged APPSWE/PS1ΔE9 murine model of Alzheimer's disease. Sci Rep 7(1):10411. https://doi.org/10.1038/s41598-017-11047-w

Minter MR, Zhang C, Leone V, Ringus DL, Zhang X, Oyler-Castrillo P, Musch MW, Liao F, Ward JF, Holtzman DM, Chang EB, Tanzi RE, Sisodia SS (2016) Antibiotic-induced perturbations in gut microbial diversity influences neuro-inflammation and amyloidosis in a murine model of Alzheimer's disease. Sci Rep 6(1):30028. https://doi.org/10.1038/srep30028

Moojen VKM, Damiani-Neves M, Bavaresco DV, Pescador BB, Comim CM, Quevedo J, Boeck CR (2012) NMDA preconditioning prevents object recognition memory impairment and increases brain viability in mice exposed to traumatic brain injury. Brain Res 1466:82–90. https://doi.org/10.1016/j.brainres.2012.05.041

Mookerjee SA, Nicholls DG, Brand MD (2016) Determining maximum glycolytic capacity using extracellular flux measurements. PLoS ONE 11(3):1–20. https://doi.org/10.1371/journal.pone.0152016

Morland C, Frøland AS, Pettersen MN, Storm-Mathisen J, Gundersen V, Rise F, Hassel B (2018) Propionate enters GABAergic neurons, inhibits GABA transaminase, causes GABA accumulation and lethargy in a model of propionic acidemia. Biochemical Journal 475(4):749–758. https://doi.org/10.1042/BCJ20170814

Morris MC (2016) Nutrition and risk of dementia: Overview and methodological issues. Ann N Y Acad Sci 1367(1):31–37. https://doi.org/10.1111/nyas.13047

Nguyen NHT, Morland C, Gonzalez SV, Rise F, Storm-Mathisen J, Gundersen V, Hassel B (2007) Propionate increases neuronal histone acetylation, but is metabolized oxidatively by glia. Relevance for propionic acidemia. J Neurochem 101(3):806–814. https://doi.org/10.1111/j.1471-4159.2006.04397.x

Norton S, Matthews FE, Barnes DE, Yaffe K, Brayne C (2014) Potential for primary prevention of Alzheimer's disease: an analysis of population-based data. Lancet Neurol 13(8):788–794. https://doi.org/10.1016/S1474-4422(14)70136-X

Nunez J (2008) Morris water maze experiment. J vis Exp 19:12–13. https://doi.org/10.3791/897

Ong L, Shah NP (2008) Influence of probiotic *Lactobacillus acidophilus* and *L. helveticus* on proteolysis, organic acid profiles, and ACE-inhibitory activity of cheddar cheeses ripened at 4, 8, and 12°C. J Food Sci. https://doi.org/10.1111/j.1750-3841.2008.00689.x

Ovalle-Magallanes B, Navarrete A, Haddad PS, Tovar AR, Noriega LG, Tovar-Palacio C, Mata R (2019) Phytomedicine Multi-target antidiabetic mechanisms of mexicanolides from *Swietenia humilis*. Phytomedicine 58:152891. https://doi.org/10.1016/j.phymed.2019.152891

Paxinos G, Franklin KBJ (2001) The mouse brain in stereotaxic coordinates, compact, third edition: the coronal plates and diagrams. http://www.amazon.com/Mouse-Stereotaxic-Coordinates-Compact-Edition/dp/0123742447?SubscriptionId=1V7VTJ4HA4

MFT9XBJ1R2&tag=mekentosjcom-20&linkCode=xm2&camp=2025&creative=165953&creativeASIN=0123742447%5Cnpapers2://publication/uuid/E9682C78-4697-4EF6-B8E9-

Perez-Cruz C, Nolte MW, Van Gaalen MM, Rustay NR, Termont A, Tanghe A, Kirchhoff F, Ebert U (2011) Reduced spine density in specific regions of CA1 pyramidal neurons in two transgenic mouse models of Alzheimer's disease. J Neurosci 31(10):3926–3934. https://doi.org/10.1523/JNEUROSCI.6142-10.2011

Perez-Nievas BG, Stein TD, Tai HC, Dols-Icardo O, Scotton TC, Barroeta-Espar I, Fernandez-Carballo L, De Munain EL, Perez J, Marquie M, Serrano-Pozo A, Frosch MP, Lowe V, Parisi JE, Petersen RC, Ikonomovic MD, López OL, Klunk W, Hyman BT, Gómez-Isla T (2013) Dissecting phenotypic traits linked to human resilience to Alzheimer's pathology. Brain 136(8):2510–2526. https://doi.org/10.1093/brain/awt171

Perriard G, Mathias A, Enz L, Canales M, Schluep M, Gentner M, Schaeren-wiemers N, Du Pasquier RA (2015) Interleukin-22 is increased in multiple sclerosis patients and targets astrocytes. J Neuroinflammation 12(119):1–18. https://doi.org/10.1186/s12974-015-0335-3

Piedra-Quintero ZL, Serrano C, Villegas-Sepúlveda N, Maravillas-Montero JL, Romero-Ramírez S, Shibayama M, Medina-Contreras O, Nava P, Santos-Argumedo L (2019) Myosin 1F regulates M1-polarization by stimulating intercellular adhesion in macrophages. Front Immunol 10:1–16. https://doi.org/10.3389/fimmu.2018.03118

Ramnani P, Costabile A, Bustillo AGR (2015) A randomised, double- blind, cross-over study investigating the prebiotic effect of agave fructans in healthy human subjects. J Nutr Sci 4(e10):1–10. https://doi.org/10.1017/jns.2014.68

Reeves PG, Suppl M (1997) Symposium: animal diets for nutritional and toxicological research components of the AIN-93 diets as improvements in the AIN-76A Diet 1, 2. Exp Biol 127:838–841

Reick C, Ellrichmann G, Tsai T, Lee DH, Wiese S, Gold R, Saft C, Linker RA (2016) Expression of brain-derived neurotrophic factor in astrocytes—beneficial effects of glatiramer acetate in the R6/2 and YAC128 mouse models of Huntington's disease. Exp Neurol 285:12–23. https://doi.org/10.1016/j.expneurol.2016.08.012

Revtovich AV, Lee R, Kirienko NV (2019) Interplay between mitochondria and diet mediates pathogen and stress resistance in caenorhabditis elegans. PLoS Genet 15(3):1–27. https://doi.org/10.1371/journal.pgen.1008011

Ricobaraza A, Cuadrado-Tejedor M, Marco S, Pérez-Otaño I, García-Osta A (2012) Phenylbutyrate rescues dendritic spine loss associated with memory deficits in a mouse model of Alzheimer disease. Hippocampus 22(5):1040–1050. https://doi.org/10.1002/hipo.20883

Rodriguez-Callejas JD, Fuchs E, Perez-Cruz C (2016) Evidence of tau hyperphosphorylation and dystrophic microglia in the common marmoset. Front Aging Neurosci 8:1–15. https://doi.org/10.3389/fnagi.2016.00315

Romo-Araiza A, Gutiérrez-Salmeán G, Galván EJ, Hernández-Frausto M, Herrera-López G, Romo-Parra H, García-Contreras V, Fernández-Presas AM, Jasso-Chávez R, Borlongan CV, Ibarra A (2018) Probiotics and prebiotics as a therapeutic strategy to improve memory in a model of middle-aged rats. Front Aging Neurosci 10(December):1–15. https://doi.org/10.3389/fnagi.2018.00416

Rosas-Arellano A, Villalobos-González JB, Palma-Tirado L, Beltrán FA, Cárabez-Trejo A, Missirlis F, Castro MA (2016) A simple solution for antibody signal enhancement in immunofluorescence and triple immunogold assays. Histochem Cell Biol 146(4):421–430. https://doi.org/10.1007/s00418-016-1447-2

Rose J, Brian C, Pappa A, Panayiotidis MI, Franco R (2020) Mitochondrial metabolism in astrocytes regulates brain bioenergetics, neurotransmission and redox balance. Front Neurosci 14(November):1–20. https://doi.org/10.3389/fnins.2020.536682

Rothhammer V, Mascanfroni ID, Bunse L, Takenaka MC, Kenison JE, Mayo L, Chao CC, Patel B, Yan R, Blain M, Alvarez JI, Kébir H, Anandasabapathy N, Izquierdo G, Jung S, Obholzer N, Pochet N, Clish CB, Prinz M, Prat A, Antel J, Q. F. (2016) Type I interferons and microbial metabolites of tryptophan modulate astrocyte activity and central nervous system inflammation via the aryl hydrocarbon receptor. Nat Med 22(6):586–597. https://doi.org/10.1007/978-1-4614-6438-9_101571-1

Sánchez-Tapia M, Aguilar-López M, Pérez-Cruz C, Pichardo-Ontiveros E, Wang M, Donovan SM, Tovar AR, Torres N (2017) Nopal (*Opuntia ficus* indica) protects from metabolic endotoxemia by modifying gut microbiota in obese rats fed high fat/sucrose diet. Sci Rep 7(1):1–16. https://doi.org/10.1038/s41598-017-05096-4

Sanmarco LM, Polonio CM, Wheeler MA, Quintana FJ (2021) Functional immune cell–astrocyte interactions. J Exp Med 218(9):1–11. https://doi.org/10.1084/jem.20202715

Sapountzis P, Gruntjes T, Otani S, Estevez J, da Costa RR, Plunkett G, Perna NT, Poulsen M (2015) The enterobacterium Trabulsiella odontotermitis presents novel adaptations related to its association with fungus-growing termites. Appl Environ Microbiol 81(19):6577–6588. https://doi.org/10.1128/AEM.01844-15

Savignac HM, Corona G, Mills H, Chen L, Spencer JPE, Tzortzis G, Burnet PWJ (2013) Prebiotic feeding elevates central brain derived neurotrophic factor, N-methyl-d-aspartate receptor subunits and d-serine. Neurochem Int 63(8):756–764. https://doi.org/10.1016/j.neuint.2013.10.006

Scarmeas N, Luchsinger JA, Mayeux R, Stern Y (2007) Mediterranean diet and Alzheimer disease mortality. Neurology 69(11):1084–1093. https://doi.org/10.1212/01.wnl.0000277320.50685.7c

Scott Schwoerer J, Clowes Candadai S, Held PK (2018) Long-term outcomes in Amish patients diagnosed with propionic acidemia. Mol Genet Metab Rep 16(June):36–38. https://doi.org/10.1016/j.ymgmr.2018.05.004

Segain JP, Raingeard de la Blétière D, Bourreille A, Leray V, Gervois N, Rosales C, Ferrier L, Bonnet C, Blottière HM, Galmiche JP (2000) Butyrate inhibits inflammatory responses through NFkappaB inhibition: implications for Crohn's disease. Gut 47(3):397–403

Segata N, Izard J, Waldron L, Gevers D, Miropolsky L, Garrett WS, Huttenhower C (2011) Metagenomic biomarker discovery and explanation. Genome Biol 12(6):R60. https://doi.org/10.1186/gb-2011-12-6-r60

Sethi KD, Ray R, Roesel RA, Carter AL, Gallagher BB, Loring DW, Hommes FA (1989) Adult-onset chorea and dementia with propionic acidemia. Neurology 39(10):1343–1345. https://doi.org/10.1212/wnl.39.10.1343

Shao Y, Ouyang Y, Li T, Liu X, Xu X, Li S, Xu G, Le W (2020) Alteration of metabolic profile and potential biomarkers in the plasma of Alzheimer⇔s disease. Aging Dis 11(6):1459–1470

Shukla S, Tekwani BL (2020) Histone deacetylases inhibitors in neurodegenerative diseases, neuroprotection and neuronal differentiation. Front Pharmacol 11(April):1–20. https://doi.org/10.3389/fphar.2020.00537

Shultz SR, MacFabe DF, Ossenkopp KP, Scratch S, Whelan J, Taylor R, Cain DP (2008) Intracerebroventricular injection of propionic acid, an enteric bacterial metabolic end-product, impairs social behavior in the rat: Implications for an animal model of autism. Neuropharmacology 54(6):901–911. https://doi.org/10.1016/j.neuropharm.2008.01.013

Singh B, Parsaik AK, Mielke MM, Erwin PJ, Knopman DS, Petersen RC, Roberts RO (2014) Association of mediterranean diet with mild cognitive impairment and Alzheimer's disease: a systematic review and meta-analysis. J Alzheimer's Dis 39(2):271–282. https://doi.org/10.3233/JAD-130830

Solfrizzi V, Frisardi V, Seripa D, Capurso C, Vendemiale G, Pilotto A, Panza F (2010) Dietary patterns and protection against Alzheimer disease and cognitive decline. Arch Neurol 67(10):1285–1286. https://doi.org/10.1001/archneurol.2010.244

Spichak S, Donoso F, Moloney GM, Gunnigle E, Brown JM, Codagnone M, Dinan TG, Cryan JF (2021) Microbially-derived short-chain fatty acids impact astrocyte gene expression in a sex-specific manner. Brain Behav Immun Health 16(June):100318. https://doi.org/10.1016/j.bbih.2021.100318

Sun J, Wang F, Li H, Zhang H, Jin J, Chen W, Pang M, Yu J, He Y, Liu J, Liu C (2015) Neuroprotective effect of sodium butyrate against cerebral ischemia/reperfusion injury in mice. Biomed Res Int. https://doi.org/10.1155/2015/395895

Sun J, Xu J, Yang B, Chen K, Kong Y, Fang N, Gong T, Wang F, Ling Z, Liu J (2020) Effect of *Clostridium butyricum* against microglia-mediated neuroinflammation in Alzheimer's Disease via regulating gut microbiota and metabolites butyrate. Mol Nutr Food Res 64(2):1–11. https://doi.org/10.1002/mnfr.201900636

Syeda T, Sanchez-Tapia M, Pinedo-Vargas L, Granados O, Cuervo-Zanatta D, Rojas-Santiago E, Díaz-Cintra S, Torres N, Perez-Cruz C (2018) Bioactive food abates metabolic and synaptic alterations by modulation of gut microbiota in a mouse model of Alzheimer's disease. J Alzheimer's Dis 66(4):1657–1682. https://doi.org/10.3233/JAD-180556

Takanaga H, Chaudhuri B, Frommer WB (2008) Glucose sensors. Biochim Biophys Acta 1778(4):1091–1099. https://doi.org/10.1201/b18990-115

Trichopoulou A, Kyrozis A, Rossi M, Katsoulis M, Trichopoulos D, La Vecchia C, Lagiou P (2015) Mediterranean diet and cognitive decline over time in an elderly Mediterranean population. Eur J Nutr 54(8):1311–1321. https://doi.org/10.1007/s00394-014-0811-z

Ulrike E, Christoph L, Katja D, Simone S, Dirk H, Markus MH, Zeitz M, Britta S, Anja AK (2014) A guide to histomorphological evaluation of intestinal inflammation in mouse models. Int J Clin Exp Pathol 7(8):4557–4576

Val-Laillet D, Guérin S, Coquery N, Nogret I, Formal M, Romé V, Le Normand L, Meurice P, Randuineau G, Guilloteau P, Malbert CH, Parnet P, Lallès JP, Segain JP (2018) Oral sodium butyrate impacts brain metabolism and hippocampal neurogenesis, with limited effects on gut anatomy and function in pigs. FASEB J 32(4):2160–2171. https://doi.org/10.1096/fj.201700547RR

Valdebenito R, Ruminot I, Garrido-Gerter P, Fernández-Moncada I, Forero-Quintero L, Alegría K, Becker HM, Deitmer JW, Barros LF (2016) Targeting of astrocytic glucose metabolism by beta-hydroxybutyrate. J Cereb Blood Flow Metab 36(10):1813–1822. https://doi.org/10.1177/0271678X15613955

Vijay N, Morris M (2014) Role of monocarboxylate transporters in drug delivery to the brain. Curr Pharm Des 20(10):1487–1498. https://doi.org/10.2174/13816128113199990462

Vikram A, Kim YR, Kumar S, Li Q, Kassan M, Jacobs JS, Irani K (2016) Vascular microRNA-204 is remotely governed by the microbiome and impairs endothelium-dependent vasorelaxation by downregulating Sirtuin1. Nat Commun 7:1–9. https://doi.org/10.1038/ncomms12565

Vogt W (1995) Oxidation of methionyl residues in proteins: tools, targets, and reversal. Free Radical Biol Med 18(1):93–105. https://doi.org/10.1016/0891-5849(94)00158-G

Walf AA, Frye CA (2007) The use of the elevated plus maze as an assay of anxiety-related behavior in rodents. Nat Protoc 2(2):322–328. https://doi.org/10.1038/nprot.2007.44

Wang L, Christophersen C, Sorich M, Gerber J, Angley M. Conlon M (2010) Gut bacterial and fermentation profiles are altered in children with autism. Gastroenterological Society of Australia, pp 1–2

Wang Y, Wang Z, Wang Y, Li F, Jia J, Song X, Qin S, Wang R, Jin F, Kitazato K, Wang Y (2018) The gut-microglia connection: Implications for central nervous system diseases. Front Immunol 9:1–16. https://doi.org/10.3389/fimmu.2018.02325

Waniewski RA, Martin DL (1998) Preferential utilization of acetate by astrocytes is attributable to transport. J Neurosci 18(14):5225–5233. https://doi.org/10.1523/jneurosci.18-14-05225.1998

Weaver D, Gupta M, Meek A, Wang Y, Wu F (2020) Alzheimer's disease as a disorder of tryptophan metabolism (2745). Neurology 94(15 Supplement):2745

Whiley L, Chappell KE, D'Hondt E, Lewis MR, Jiménez B, Snowden SG, Soininen H, Kłoszewska I, Mecocci P, Tsolaki M, Vellas B, Swann JR, Hye A, Lovestone S, Legido-Quigley C, Holmes E (2021) Metabolic phenotyping reveals a reduction in the bioavailability of serotonin and kynurenine pathway metabolites in both the urine and serum of individuals living with Alzheimer's disease. Alzheimer's Res Therapy 13(1):1–18. https://doi.org/10.1186/s13195-020-00741-z

Wu L, Han Y, Zheng Z, Peng G, Liu P, Yue S, Zhu S, Chen J, Lv H, Shao L, Sheng Y, Wang Y, Li L, Li L, Wang B (2021) Altered gut microbial metabolites in amnestic mild cognitive impairment and alzheimer's disease: Signals in host–microbe interplay. Nutrients 13(1):1–15. https://doi.org/10.3390/nu13010228

Wyss MT, Magistretti PJ, Buck A, Weber B (2011) Labeled acetate as a marker of astrocytic metabolism. J Cereb Blood Flow Metab 31(8):1668–1674. https://doi.org/10.1038/jcbfm.2011.84

Xiao Q, Yan P, Ma X, Liu H, Perez R, Zhu A, Gonzales E, Burchett JM, Schuler DR, Cirrito JR, Diwan A, Lee JM (2014) Enhancing astrocytic lysosome biogenesis facilitates Aβ clearance and attenuates amyloid plaque pathogenesis. J Neurosci 34(29):9607–9620. https://doi.org/10.1523/JNEUROSCI.3788-13.2014

Xin Y, Diling C, Jian Y, Ting L, Guoyan H, Hualun L, Xiaocui T, Guoxiao L, Ou S, Chaoqun Z, Jun Z, Yizhen X (2018) Effects of oligosaccharides from morinda officinalis on gut microbiota and metabolome of APP/PS1 transgenic mice. Front Neurol 9:1–14. https://doi.org/10.3389/fneur.2018.00412

Yilmaz A, Geddes T, Han B, Bahado-Singh RO, Wilson GD, Imam K, Maddens M, Graham SF (2017) Diagnostic biomarkers of Alzheimer's disease as identified in saliva using 1H NMR-based metabolomics. Journal of Alzheimer's Disease 58(2):355–359. https://doi.org/10.3233/JAD-161226

Yusufov M, Weyandt LL, Piryatinsky I (2017) Alzheimer's disease and diet: a systematic review. Int J Neurosci 127(2):161–175. https://doi.org/10.3109/00207454.2016.1155572

Zeng MY, Inohara N, Nuñez G (2017) Mechanisms of inflammation-driven bacterial dysbiosis in the gut. Physiol Behav 10(1):18–26. https://doi.org/10.1038/mi.2016.75.Mechanisms

Zhang C, Brandt MJ, Schwab C, Gänzle MG (2010) Propionic acid production by cofermentation of *Lactobacillus buchneri* and *Lactobacillus diolivorans* in sourdough. Food Microbiol 27(3):390–395. https://doi.org/10.1016/j.fm.2009.11.019